International Journal of Biological Macromolecules 370 (2026) 152828

Contents lists available at ScienceDirect

International Journal of Biological Macromolecules

journal homepage: www.elsevier.com/locate/ijbiomac

A multifunctional adhesive antibacterial chitosan/hyaluronic acid hydrogel enabling sustained release of human umbilical cord mesenchymal stem cell-derived exosomes for accelerated full-thickness skin repair

Zhonghua Luo [a,1], Zhiquan Hou [a,1], Mi Wu [b], Yan Zhao [b], Fuhai Hui [c], Yudong Wu [a], Yuan Wang [a,*], Yunen Liu [a,*]

[a] School of Shuren International, Shenyang Medical College, Liaoning Provincial Key Laboratory of Skin, Mucosa and Soft Tissue Trauma Repair and Reconstruction, Shenyang Municipal Key Laboratory of Digestive System Injury Repair and Reconstruction, No. 146, Huanghe North Street, Shenyang, 110034, China
[b] Jihua Laboratory, Foshan, Guangdong, China
[c] Shenyang Pharmaceutical University, Shenyang, Liaoning, China

ARTICLE INFO

Keywords:
Chitosan
Hyaluronic acid
Exosomes
Wound healing
Angiogenesis

ABSTRACT

Promoting skin wound healing is a major global public health challenge. Stem cell exosomes are regarded as a promising and ideal therapeutic approach. However, effective stem cell exosome therapy also depends on suitable vectors to promote the release and stability of exosomes. In this study, exosomes derived from human umbilical cord mesenchymal stem cells (UCMSCs-exo) were loaded into crosslinked hydrogels of chitosan (CS) and hyaluronic acid (HA) to prepare a novel multifunctional hydrogel dressing with sustained release of exosomes (UCMSCs-exo@CS-HA). The UCMSCs-exo@CS-HA hydrogels had good properties, including three-dimensional porous structure, exosomes loading performance, mechanical properties, tissue adhesion, antibacterial activity, degradation performance, and good biocompatibility. The whole skin defect model of mice verified that the UCMSCs-exo@CS-HA hydrogels reduced the expression level of inflammatory factor cyclooxygenase-2 (COX2) and inducible nitric oxide synthase (iNOS), promoted the orderly deposition of collagen and angiogenesis, and effectively promoted wound healing. Overall, the UCMSCs-exo@CS-HA hydrogels can effectively regulate the interaction between inflammation, tissue fibrosis, and angiogenesis, providing a promising solution for the treatment of skin injury.

1. Introduction

The skin is the largest organ in the human body, which consists of the epidermis, dermis, and subcutaneous tissue, and plays a crucial role in defending the body against the invasion of pathogens [1]. Skin tissue damage caused by external factors is called a wound. Wound healing is a common problem within clinical settings. It is difficult, time-consuming, and expensive. Moreover, it seriously harms a person's physical and mental health, reduces their quality of life, and increases the burden on families and society by consuming healthcare resources [2]. Traditional wound healing therapy includes wound negative pressure therapy, gauze dressing, and hyperbaric oxygen therapy. However, these treatment methods may lead to secondary injuries and limited tissue movement, which cannot meet the needs of patients [3]. Therefore, designing and developing an effective wound-healing therapy has become a major research goal.

Keeping the wound moist can reduce the risk of wound infection, reduce complications, and promote healing [4]. In recent years, hydrogel dressings have been widely used in wound treatment for excellent moisturizing properties and three-dimensional porous structure [5]. Recent studies on antibacterial hydrogels and microenvironment-feedback hydrogels have further emphasized that wound dressings should not only maintain moisture but also match infection-, inflammation-, and repair-related cues in the wound microenvironment [6,7]. Hydrogels are classified according to crosslinking methods, which mainly include chemical crosslinking and physical crosslinking. Chemically crosslinked hydrogels have superior structural properties and are more stable than physically crosslinked hydrogels,

* Corresponding authors.
E-mail addresses: 1483345395@qq.com (Y. Wang), liuye990116@163.com (Y. Liu).
[1] These authors contributed equally to this work.

https://doi.org/10.1016/j.ijbiomac.2026.152828
Received 10 March 2026; Received in revised form 20 May 2026; Accepted 29 May 2026
Available online 1 June 2026

but their application and development in biomedical and other fields are limited by reactions that are harmful to biological activity [8]. In contrast, physically cross-linked hydrogels form three-dimensional networks through non-covalent interactions without the need for chemical cross-linkers, thereby offering superior biocompatibility [9]. Its cross-linking process is reversible and can undergo dissociation under specific environmental stimuli, which gives it unique advantages in biomedical applications [9].

Polysaccharides are one of the common matrix components of physically cross-linked hydrogels that provide a physical barrier to wounds [10]. Chitosan (CS) is a polysaccharide widely found in nature [11]. The CS is abundant in the shells of shrimp, crabs, and other arthropods, as well as in the cell walls of lower plants [12]. The CS has good biocompatibility, is easy to form films, and has antibacterial and antioxidant properties. Therefore, it has been intensively researched and widely applied in biomedical applications, for example as a drug carrier or dressing [13]. However, the CS has some limitations, including poor stability, limited solubility, and difficulty in dissolving under neutral and alkaline conditions [14]. Hyaluronic acid (HA) is an important component of the extracellular matrix. It is a naturally occurring non-sulfur polymeric polysaccharide [15]. As a signal transduction molecule, the HA can be involved in cell signaling, including cell proliferation and migration, by binding the receptor CD44 and interacting with various proteins in the extracellular matrix and cell membrane [16,17]. The HA is non-antigenic, highly absorbent, viscoelastic, and biocompatible. However, the HA is susceptible to degradation, is relatively unstable, and has a short half-life [18]. In order to solve the limitation of the regulation of physical and chemical properties of a single material. Li et al. prepared a composite hydrogel with the CS and the HA for wound healing [19]. However, the composite hydrogel has no anti-inflammatory activity, so it can be obtained by loading drugs.

Related literature reports that pluripotent stem cells also play an important role in tissue repair processes [20]. Mesenchymal stem cells (MSCs) derived from mesoderm have become the mainstream of wound-healing research owing to their high self-renewal capability and multi-directional differentiation potential. Compared with adult mesenchymal stem cells, umbilical cord mesenchymal stem cells (UCMSCs) have obvious advantages, namely good self-renewal ability, pluripotent differentiation characteristics, and lower immunogenicity [21]. In addition, umbilical cord mesenchymal stem cell exosomes (UCMSCs-exo) have received considerable attention in the field of wound-healing research. UCMSCs-exo are extracellular vesicles that assist in intercellular communication, cellular differentiation, and proliferation, which also promote angiogenesis and immune signaling [22]. Moreover, UCMSCs-exo can control the immune response, inhibit the expression of inflammatory factors, and reduce proliferative scar formation during wound healing [23]. However, the application of UCMSCs-exo to wound repair remains a major challenge in clinical applications owing to the rapid in vitro clearance of UCMSCs-exo, which may affect their function, and the low retention of UCMSCs-exo in vivo [24]. Song et al. have demonstrated that the use of novel biocompatible dressings as slow-release carriers for exosomes can maintain the biological activity of exosomes in the wound and further promote wound healing [25].

In this study, it was assumed that the chitosan/hyaluronic acid hydrogels as a functional carrier can efficiently load and release the UCMSCs-exo. The incorporation of UCMSCs-exo into the CS-HA hydrogel delivery system is mainly based on the following basic principles. Firstly, the stability issue of UCMSCs-exo in in vivo applications has been resolved. UCMSCs-exo is prone to degradation by enzymes and clearance by the immune system in the in vivo environment, resulting in a decrease in its bioavailability. The encapsulation effect of the hydrogels can protect exosomes from adverse factors in vivo, and improve its stability and bioavailability in vivo [26]. Secondly, the targeted delivery of exosomes at the local wound site has been achieved [26]. This UCMSCs-exo@CS-HA hydrogels was more effective in regulating inflammatory responses, promoting angiogenesis and granulation tissue formation, and accelerating epithelial regeneration in a mouse model of full-thickness skin defects.

As a result, it significantly surpasses the use of hydrogels or exosomes alone, achieving faster and higher-quality wound healing. Therefore, we constructed the CS-HA hydrogels delivery system by physical cross-linking CS and HA in this study. Next, the UCMSCs-exo with strong anti-inflammatory effect was loaded on the CS-HA hydrogels to construct a new delivery system of the UCMSCs-exo@CS-HA wound repair hydrogels. The physicochemical properties, biosafety and biological application of the UCMSCs-exo@CS-HA hydrogels as a sustainable wound drug delivery system were systematically studied. We then analyzed the UCMSCs-exo@CS-HA hydrogels to evaluate its anti-inflammatory and antibacterial activity, tissue regeneration capability, vascular regeneration capability, and wound-healing safety. Furthermore, we investigated the mechanism by which the UCMSCs-exo@CS-HA hydrogels promotes wound healing.

2. Materials and methods

2.1. Materials

The CS (Mean molecular weight (M_w) of 62 × 10^4, degree of deacetylation = 84% determined by acid-base titration) was provided by China National Pharmaceutical Group Chemical Reagent Co. The HA (molecular weight: 1500–2500 kDa) was purchased from China Pharmaceutical Group Chemical Reagent Co. The BCA protein kit was obtained by Hangzhou Fode Biotechnology Co. PBS buffer solution, 4% paraformaldehyde fixative and serum-free cell cryopreservation solution were purchased from Beijing Lanjieke Technology Co. Isoflurane was provided by Shanghai Macklin Biochemical Technology Co. CD31, VEGF, and HIF1-α antibodies were purchased from Shanghai Abbot Anti Trading Co. Exosome fluorescent labeling dye (DiR) and exosome red fluorescent labelling dye (PKH26) were supplied by Shanghai Umibio Science and Technology Co. MEM medium and fetal bovine serum were bought from Shanghai Darthel Bio-technology Co. Ltd. MEM medium and fetal bovine serum were purchased from Shanghai Darthelm Bioscience Co. Trypsin was obtained by Shanghai Univision Biotechnology Co. The cell counting kit and CCK-8 were purchased from Beijing Solepol Technology Co.

2.2. Preparation and characterization of the UCMSCs-exo

2.2.1. Preparation of the UCMSCs-exo

The USMCs-exo was purchased from Xi'an Chuyuan Cel Biotechnology Co., LTD., and stored in a −80 °C refrigerator. The concentrations of the UCMSCs-exo were determined by the BCA protein kit [27]. The morphology of exosomes was analyzed by transmission electron microscopy (TEM, 8-H7650, China). Finally, the signature markers CD9 (1:6000, Proteintech, China), CD63 (1:1000, Proteintech, China) and TSG101 (1:500, Proteintech, China) of the UCMSCs-exo were analyzed by protein blotting assay.

2.2.2. Exosome fluorescence labeling PKH staining

The PKH26 staining kit was used to prepare the exosome dye working solution. 100 μL dye working solution was added to 500 μg exosomes. After incubation, unbound dyes are removed by centrifugation. The stained exosomes were obtained by suspension precipitation of 200 μL PBS buffer solution [28]. The expression of UCMSCs-exo was observed at 24 h, 48 h, and 72 h, respectively.

2.3. Preparation and characterization of the CS-HA hydrogels

2.3.1. Preparation of the CS-HA hydrogels

The structural characterization of CS and HA has been shown in our previous studies [29]. It should be clarified that dry CS and HA powders were not directly mixed to instantly generate a hydrogel. In the actual

preparation process, 5.85 g of CS powder was first dispersed in 60 g of sterile saline, followed by addition of 1.65 g of 0.5% (*w/v*) acetic acid under continuous stirring at room temperature. The weakly acidic medium protonated the amino groups of CS and promoted polymer-chain hydration, thereby producing a uniform CS solution/gel precursor. Subsequently, 6 g of HA powder was slowly added and stirred until a homogeneous CS-HA hydrogel was formed (Fig. 1). The hydrogel network was generated mainly by electrostatic interactions between protonated CS amino groups and HA carboxylate groups, together with hydrogen bonding among amino, hydroxyl, and carboxyl groups. The final hydrogel pH was checked using a calibrated pH meter and maintained at 6.8 ± 0.2 before subsequent biological experiments. Together with the hemolysis, cell viability, and subcutaneous implantation results, this near-neutral pH supported the absence of obvious acid-related irritation under the present experimental conditions.

2.3.2. Rheological property test

Subsequently, rheological experiments were carried out to assess the physical properties of the CS-HA hydrogels using a hybrid rheometer equipped with parallel plates (direct diameter 37 mm). The CS-HA hydrogels was thoroughly mixed and loaded onto a preheated carrier table. For dynamic frequency scanning, the frequency was set to 0.1–100 rad/s and the strain was maintained at 1%. The frequency was set from 0.01 Hz to 100 Hz for viscosity scanning and shear viscosity scanning [30].

2.3.3. Fourier infrared spectrum of the CS-HA hydrogels

The infrared spectra of CS, HA, and the CS-HA hydrogels were tested by a Fourier transform infrared spectrometer (Tensor 27, Bruker, Billerica, USA) with a wave number scanning range of 4000 cm^{-1}-400 cm^{-1}.

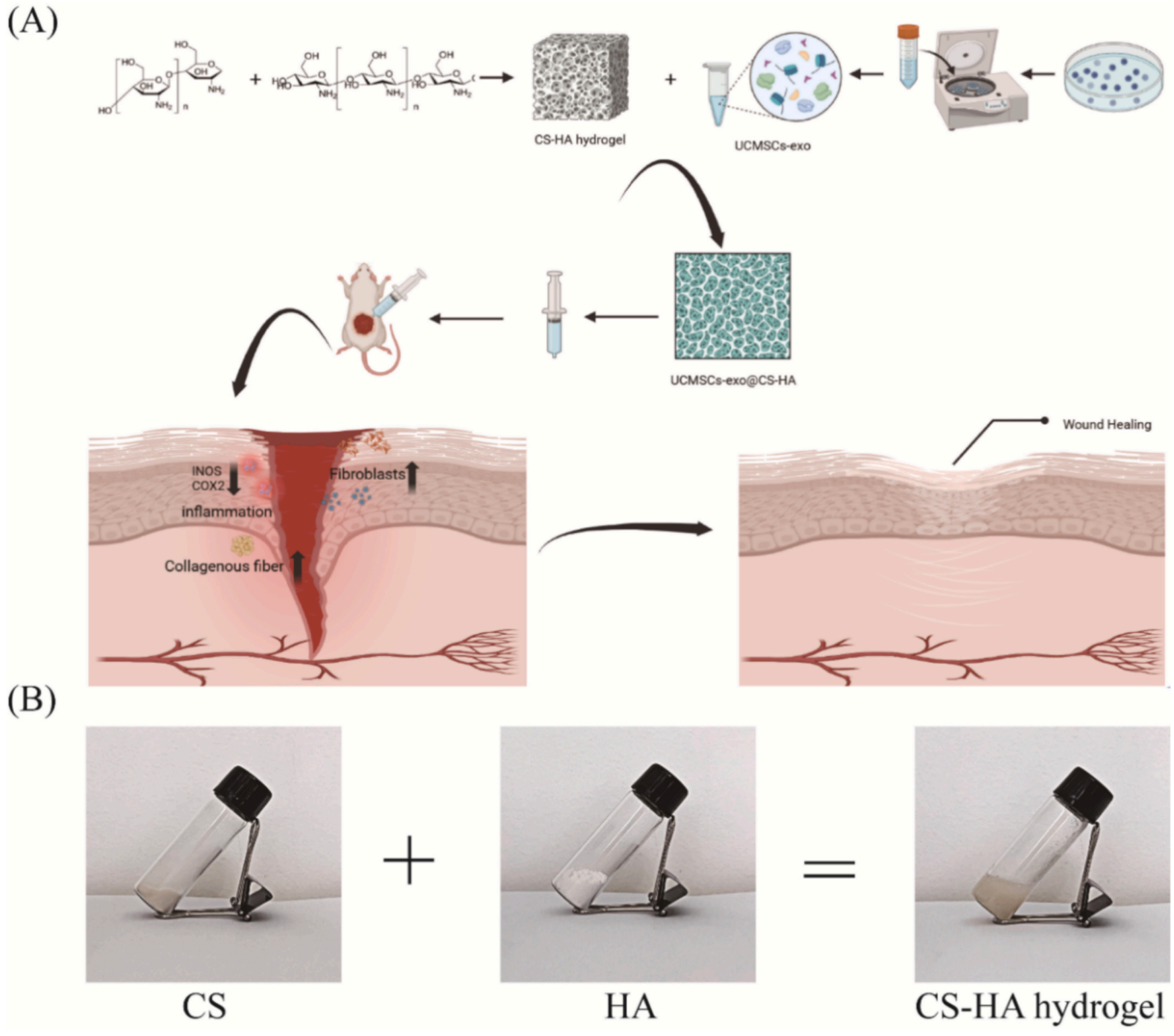

Fig. 1. (A) Schematic illustration of the preparation of human umbilical cord mesenchymal stem cell-derived exosome-loaded chitosan/hyaluronic acid hydrogel (UCMSCs-exo@CS-HA). (B) Preparation diagram of the chitosan/hyaluronic acid hydrogel (CS-HA hydrogel). Chitosan powder was dispersed in dilute acetic acid/saline to protonate amino groups, followed by addition of hyaluronic acid powder; the hydrogel network was formed mainly through electrostatic interactions between protonated chitosan amino groups and hyaluronic acid carboxylate groups, together with hydrogen bonding and physical chain entanglement.

2.3.4. The CS-HA hydrogels adhesion test

The experimental animals and protocol have been approved by the Animal Protection and Ethics Committee of Shenyang Medical College (SYYXY2023030501). We tested the hydrogel's ability to adhere to biological tissues by examining mouse visceral tissues as well as pig skin.

2.3.5. Haemolysis test and assessment of swelling properties

The blood compatibility of the hydrogels was evaluated using an in vitro hemolysis assay [31]. Fresh anticoagulated whole blood was washed by centrifugation with an appropriate amount of PBS, and the resulting precipitate was mixed with PBS in a certain proportion to obtain the erythrocyte suspension. 20 mg of hydrogels samples were added with 200 μL of RBC suspension and 800 μL of PBS, and incubated at 37 °C for 1 h. Experimental samples and control samples were incubated under the same conditions. All samples were centrifuged at 5000 r/min for 5 min, and the absorbance value of the supernatant at 540 nm was determined by using the enzyme marker, and the hemolysis rate of the samples was calculated based on the absorbance value. Then the hydrogel was immersed in PBS solution at 37 °C (pH = 7.4) and weighed at a fixed time [32]. The swelling property of the hydrogel was determined by the specific gravity method. The calculation formula is as follows: where Qt is the quality of the hydrogel after swelling, Q0 is the mass of the hydrogel before swelling.

$$\text{Hemolysis rate } (\%) = \frac{OD_{sample} - OD_{PBS}}{OD_{ddh_2O} - OD_{PBS}} \times 100\%$$

$$\text{Swelling rate } (\%) = \frac{Q_t - Q_0}{Q_0} \times 100\%$$

2.4. In vivo biocompatibility and preliminary degradation-related evaluation of hydrogels

The experimental animals and protocol have been approved by the Animal Protection and Ethics Committee of Shenyang Medical College (SYYXY2023030501). The rats were anesthetized with 1.5% isoflurane, and the hydrogel was implanted under the skin of the back of the rats. This subcutaneous implantation assay was used primarily to evaluate local tissue compatibility and to provide preliminary histological evidence related to hydrogel degradation in vivo. HE staining was used to detect tissue inflammation on the 7th and 14th day after implantation. Because direct residual hydrogel morphology, volume, or mass loss was not quantitatively tracked over time, these data were not interpreted as a complete in vivo degradation assay.

2.5. Preparation of the UCMSCs-exo@CS-HA hydrogels

Before exosome loading, the prepared CS-HA hydrogels were sterilized by brief ultraviolet irradiation (6.9 mW/cm^2, 360–480 nm) for 10 s. The sterile CS-HA hydrogels were then mixed proportionally with UCMSCs-exo in a centrifuge tube and gently centrifuged for 3 min to ensure that UCMSCs-exo was evenly distributed in the gel. No photoinitiator was added, and no UV-triggered covalent crosslinking reaction was designed in this system. Thus, ultraviolet exposure functioned as a brief sterilization step rather than a hydrogel-forming or exosome-crosslinking reaction. The UCMSCs-exo@CS-HA hydrogels were maintained by the preformed physically crosslinked CS-HA network and by non-covalent interactions between the polymer network and UCMSCs-exo. This non-covalent loading strategy is consistent with previously reported exosome-loaded hydrogel systems designed for local extracellular-vesicle retention [33].

2.6. In vitro release of UCMSCs-exo

In vitro release of UCMSCs-exo was investigated using a transwell chamber rather than a dialysis bag [24]. The transwell system was selected because it keeps the hydrogel in a defined upper compartment without compression or deformation, reduces possible adsorption or retention of nanoscale extracellular vesicles by dialysis membranes, and more closely mimics diffusion from a wound dressing into wound exudate. The labeled UCMSCs-exo@CS-HA was placed in the upper chamber of the transwell on a 24-well plate, and 1.2 mL of release medium (PBS solution containing 10% fetal bovine serum) was added to the lower chamber. The transwell plate was placed in an orbital shaker at 37 °C and shaken at 60 rpm. At the predetermined time point, 400 μL of the chamber solution was removed and promptly replenished with fresh release medium. The fluorescence intensity of the samples was measured at 488 nm as the excitation wavelength and 525 nm as the emission wavelength, and the cumulative release rate was calculated.

2.7. Small animal live imaging

The exosomal fluorescent dye (DiR) was diluted with PBS buffer solution to prepare a dye-working solution with a concentration of 100 μM. The centrifuge tube containing the mixture was removed and centrifuged at 9500 rpm for 60 min at 4 °C and the supernatant was discarded. Then, PBS was added for resuspension and the labeled UCMSCs-exo was obtained by centrifugation at 12,400 rpm at 4 °C for 2 min [34]. The experiments were approved by the Ethics Committee of the Laboratory Animal Research Centre of Shenyang Medical College (protocol no. SYYXY2023030501). The C57BL/6 mice weighing 18–22 g were anesthetized with isoflurane to establish a model of total skin defects. Dir-labeled UCMSCs-exo and the UCMSCs-exo@CS-HA hydrogels were applied to the traumas on the back of the mice. Fluorescence changes on the back of mice were detected by a small animal live imaging instrument (Aniview 600, GuangZhou, China).

2.8. Biocompatibility of the UCMSCs-exo@CS-HA hydrogels

The L929 cells were inoculated into 24-well plates and cultured for 24 h at 37 °C in a cell culture incubator. Afterward, they were co-cultured with the UCMSCs-exo, the CS-HA hydrogels, and the UCMSCs-exo@CS-HA hydrogels. The operation was carried out using a live/dead staining kit, and the green fluorescence intensity inside the cells was observed using a fluorescence microscope [35,36].

2.9. Cellular experiments

2.9.1. Cell proliferation assay

The fibroblasts were inoculated into 96-well plates (biologix, Beijing), with approximately 1 × 103 cells per well [37]. After cell adhesion, the UCMSCs-exo at concentrations of 2, 5, and 10 μg/mL were added to the medium and incubated at 37 °C. At 24 h, 48 h, and 72 h of incubation, after removing the medium, 100 μL of medium containing 10% CCK-8 reagent (Solepol, China) was added to each well, and incubated at 37 °C for 4 h. The absorbance value of each well at 450 nm was measured by the multifunctional enzyme-labeled substance [38]. The calculation formula was as follows.

$$\text{Cell proliferation rate } (\%) = \frac{OD_{treatment} - OD_{control}}{OD_{control}} \times 100\%$$

2.9.2. Cytotoxicity assay

The fibroblasts were incubated in a 5% CO2 incubator at 37 °C for 24 h. After incubation, the UCMSCs-exo was diluted equally to 10, 20, and 40 μg/mL, and four replicate wells of 100 μL/well were set up for each concentration gradient [39,40]. Absorbance values at 450 nm were read by enzyme markers. The formula for the cytotoxicity assay was as follows.

$$\text{Cell cytotoxicity rate } (\%) = \frac{OD_{treatment} - OD_{blank}}{OD_{control} - OD_{blank}} \times 100\%$$

2.9.3. Cell scratch test

The L929 cells were inoculated into a 6-well plate at a density of 5×10^5 per well and cultured for 24 h. Then, a straight line was drawn vertically in the middle area of each well with a 200 μL gun tip. Then the UCMSCs-exo, the CS-HA hydrogels, and the UCMSCs-exo@CS-HA hydrogel were scribed in each well separately, and the wells without drug intervention were set as control. The changes in the scratched area of each group were observed by microscope and photographed at 0 h and 24 h, respectively. The scratch area of each group at 0 h and 24 h was measured using Image-J software. The calculation formula was as follows, where W0 represented the initial scratch width, and Wt represented the scratch width after the experiment.

$$\text{Cell scratch healing rate } (\%) = \frac{W_0 - W_t}{W_0} \times 100\%$$

2.10. Antibacterial experiment

The in vitro antibacterial ability of UCMSCs-exo@CS-HA hydrogels was evaluated using *Escherichia coli* (*E. coli*, ATCC 25922) and *Staphylococcus aureus* (*S. aureus*, ATCC 25923). In short, the bacteria were taken out from −80 °C and thawed for passage. The passage was performed at least three times to prepare a bacterial suspension. The concentration of the bacterial suspension was measured using a turbidimeter, and the bacterial concentration was 0.5 McFarland. LB agar plates were used to culture bacteria at pH 7.0 ± 0.2 (Qingdao Haibo Biotechnology Co.). For each bacterial strain, the experiment included four treatment groups: control, UCMSCs-exo, CS-HA hydrogels, and UCMSCs-exo@CS-HA hydrogels. Thus, a total of eight bacteria-treatment combinations were evaluated. The concentration of UCMSCs-exo was 10 μg/mL, and the amount of hydrogel was 100 μL per well. After incubation for 2 h, the samples were resuspended with 1 mL sterile PBS buffer solution and added to the bacterial culture medium for 24 h. Subsequently, bacterial colonies were counted using ImageJ. Finally, the antibacterial rate was calculated using the following formula: antibacterial rate = (number of colonies in the control group − number of colonies in the experimental group) / number of colonies in the control group × 100%.

2.11. Animal experimentation

2.11.1. Establishment of animal models

In vivo procedures were approved by the Ethics Committee of Experimental Animal Research Centre, Shenyang Medical College (protocol No. SYYXY2023030501) and conducted by the European regulation on the care and use of animals in experimental procedures and the ARRIVE guidelines. The male C57BL/6 mice with body weights of 18–22 g were adaptive feeding for 7 days. The ability of UCMSCs-exo@CS-HA to promote wound healing was evaluated by establishing a full-thickness skin injury model in mice. Forty mice were randomly divided into four groups, namely the control group, the CS-HA hydrogels group, the UCMSCs-exo group and the UCMSCs-exo@CS-HA hydrogels group, with 10 mice in each group. On the 0, 3, 5, 7, 9 and 10 days, each mouse was photographed with a camera at the same height and angle. Image-J software was used to measure and analyze the wound area and calculate the wound healing rate.

2.11.2. Histological analysis and immunohistochemistry

The cut wound skin of mice was fixed with 4% paraformaldehyde, dehydrated and embedded, and cut into 3–5 μm thick pathological sections for HE staining. Masson staining was used to determine the amount and maturity of collagen in the wound bed. The proportion of collagen was calculated using Image-Pro Plus 6.0 software [34]. Immunohistochemical staining (IHC) was then performed, and the collected sections were deparaffinized and rehydrated [41]. To assess the vascularisation of the wound tissue, tissue sections were first reacted with primary antibodies against CD31 (1:100, Abcam, China), VEGF (1:1000, Abcam, China), and HIF1-α (1:250, Abcam, China). Next, the color was developed with a chromogenic diaminobenzidine (DAB) substrate. Images of the stained sections were obtained by light microscopy.

2.12. Western blot analysis

The tissues were ground into a homogenate by placing them in a buffer containing protease and protease inhibitors. The total protein concentration was determined using a BCA kit (Beyotime, Beijing) [42]. The proteins were loaded on sodium dodecyl sulfate-polyacrylamide gel electrophoresis. Transfer of isolated proteins to polyvinylidene fluoride membranes, PVDF membranes were closed with skimmed milk powder at 37 °C for 1 h and then incubated with primary antibody overnight at 4 °C. PVDF membranes were then incubated with secondary antibodies for 1 h, followed by the application of an enhanced chemiluminescence (ECL) kit (Thermo Fisher, Zhejiang).

2.13. Statistical analysis

All the experiments were repeated three times in parallel. The data were reported as mean ± standard deviation (SD). The data were analyzed for significant differences using one-way analysis of variance (ANOVA) and *t-tests*, and differences between groups were considered significant when $p < 0.05$.

3. Results and discussion

3.1. Preparation and characterization of the UCMSCs-exo and the CS-HA hydrogels

The UCMSCs-exo were obtained from a commercial source and subsequently characterized. They were characterized by TEM and western blot analysis. The electron microscopy indicated that the UCMSCs-exo were circular or elliptical in shape (Fig. 2A). The western blot results indicated positive expression of TSG101, CD9, and CD63 exosomes markers (Fig. 2B). This was consistent with previously reported results [24]. We determined the size of the UCMSCs-exo using a nanoparticle analyzer, they were predominantly between 50 and 100 nm (Fig. 2C). In addition, PKH staining for UCMSCs-exo was further characterized (Fig. 2D). Compared with the results of 24 h and 48 h staining, the fluorescence of UCMSCs-exo at 72 h was diminished, which was considered to be caused by a rapid in vitro clearance rate and short half-life of the UCMSCs-exo [24].

The SEM indicated that the CS-HA hydrogels had an interconnected three-dimensional microporous structure (Fig. 2E). Studies have demonstrated that the three-dimensional and porous structures of the CS-HA hydrogels facilitate cell migration and growth during wound healing [43]. Meanwhile, the CS-HA hydrogels have a three-dimensional porous network structure similar to that of a natural extracellular matrix, which can provide a framework for drug delivery [43]. The results in Fig. 2F-I indicated the elastic behavior and morphological characteristics of the CS-HA hydrogels as well as the adhesion properties to pig skin and visceral tissues. Ideal hydrogel dressings should have excellent adhesion properties, which can effectively fill irregular wounds, improve wound closure, as well as prevent secondary wound infections [44]. As indicated in Fig. 2H-I, the CS-HA hydrogels had obvious tissue adhesion to pig skin and different internal organs of mice. The above results may be due to the hydrogen bond interaction between CS and HA, which makes it have good adhesion ability. Simultaneously, the amino and hydroxyl groups on the CS molecular chain form hydrogen bonds with the carboxyl group on the HA molecular chain. This intermolecular interaction enhances the network structure of the hydrogel and thus improves its tensile properties [14]. Hematocompatibility is

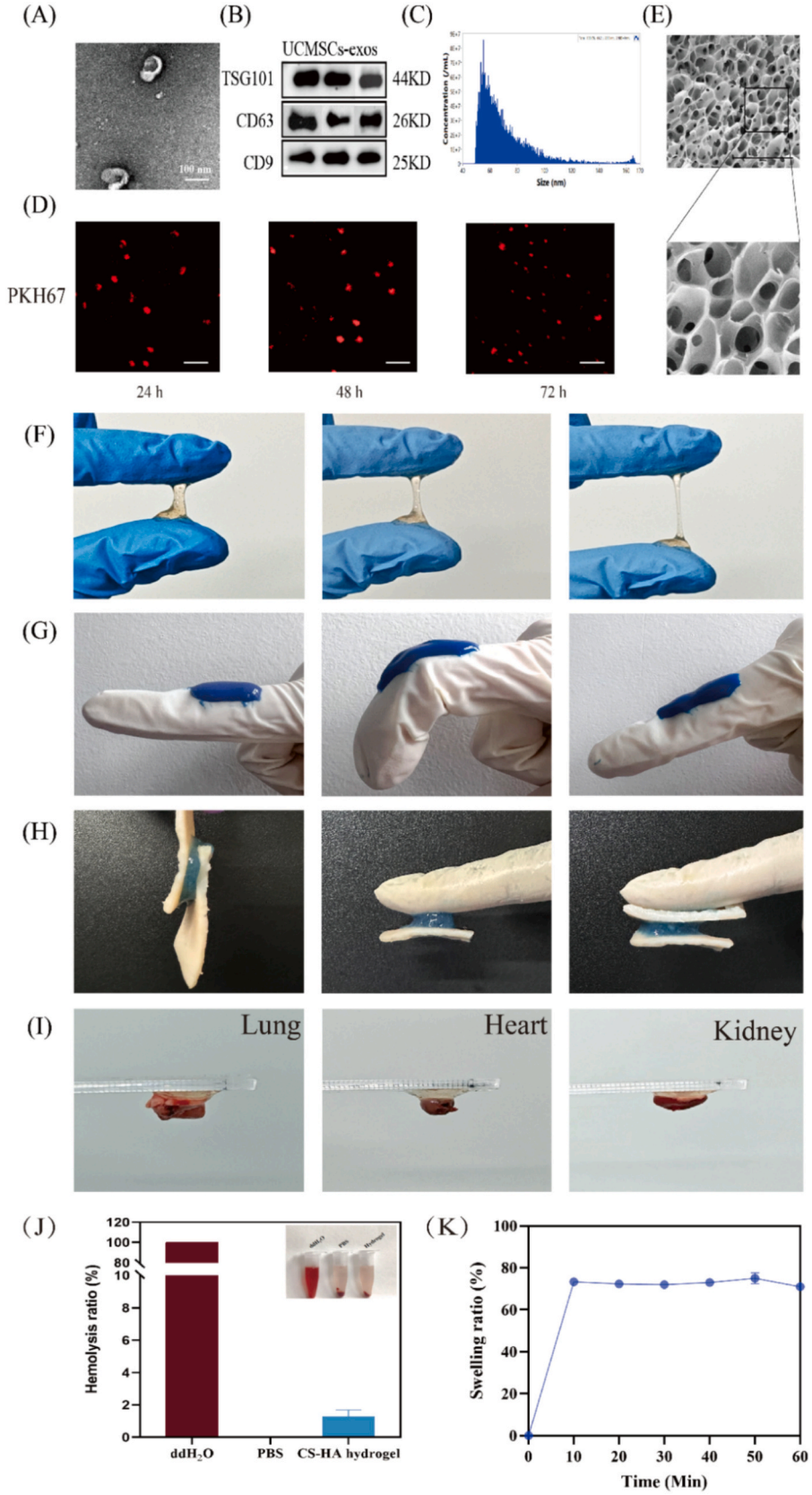

Fig. 2. Characterization of human umbilical cord mesenchymal stem cell-derived exosomes (UCMSCs-exo) and physicochemical properties of the chitosan/hyaluronic acid hydrogel (CS-HA hydrogel). (A) Transmission electron microscopy (TEM) image of UCMSCs-exo, scale bar = 100 nm. (B) Western blot analysis of exosomal markers CD9, CD63 and tumor susceptibility gene 101 protein (TSG101) ($n = 3$). (C) Particle-size distribution of UCMSCs-exo. (D) PKH26-labeled UCMSCs-exo observed by fluorescence microscopy (original magnification, 200×). (E) Scanning electron microscopy (SEM) image showing the porous microstructure of the

CS-HA hydrogel. (F-I) Digital images showing elasticity, tissue adhesion and macroscopic morphology of the CS-HA hydrogel. (J) Hemolysis evaluation of the CS-HA hydrogel. (K) Swelling behavior of the CS-HA hydrogel. Data are presented as mean +/− standard deviation where applicable.

one of the important indicators for evaluating biomedical materials. As displayed in the result Fig. 2J, compared with the positive control, the supernatant of the hydrogel samples was close to the PBS negative control, and both illuminated a clearer and lighter yellow color, indicating good blood compatibility. The hemolysis rate of the CS-HA hydrogels were 0.1%, which was below the critical safe range for hemolysis (5%). The great blood compatibility of the CS-HA hydrogels can be attributed to the fact that the negative charge carried by HA is repulsive to the negative charge of platelets thereby reducing platelet adhesion and aggregation [45]. In addition, we performed swelling experiments to evaluate the swelling behavior of the CS-HA hydrogels. As shown in Fig. 2K, the swelling of the hydrogel was a relatively slow process. In the beginning, the CS-HA hydrogels swelled faster. Water molecules penetrated the polymer network rapidly, and with the increase of time, the swelling rate curve of the hydrogel tended to slow down and reach the swelling equilibrium. The hydrogel in the swelling equilibrium state has excellent biocompatibility and biodegradability, which makes it important for applications in tissue engineering, drug transport, and cell culture [46]. Good biocompatibility specifically refers to the high level of safety and functionality that CS-HA hydrogels exhibit when interacting with biological systems.

The FTIR spectra of the CS-HA hydrogels samples were illustrated in Fig. 3A. The peaks at 1610 cm^{-1} and 1406 cm^{-1} corresponded to the carboxyl groups of the HA. The spectral bands at 1540 cm^{-1} and 1646 cm^{-1} respectively corresponded to the vibration modes of the CS amide II and amide III. It is worth noting that the amide I (C═O stretching) peak, which is usually located in the range of 1640–1660 cm^{-1}, only displays an extremely weak acromion at 1646 cm^{-1}, indicating that the degree of deacetylation (DD) of the CS is extremely high and the residual acetyl groups are quite few. Concurrently, in the infrared spectrum of the CS-HA hydrogels, the amino peak of the CS and the carboxylate peak of the HA remain discernible, with no new characteristic amide bond peak emerging. This indicated that the two formed a physical cross-linking network via electrostatic interactions and hydrogen bonds, without the generation of new covalent bonds (such as amide or ester bonds). Furthermore, the broadening of the O—H stretching vibration peak (~3400 cm^{-1}) further supported the mechanism of physically cross-linked networks enhanced by hydrogen bonding. The research of

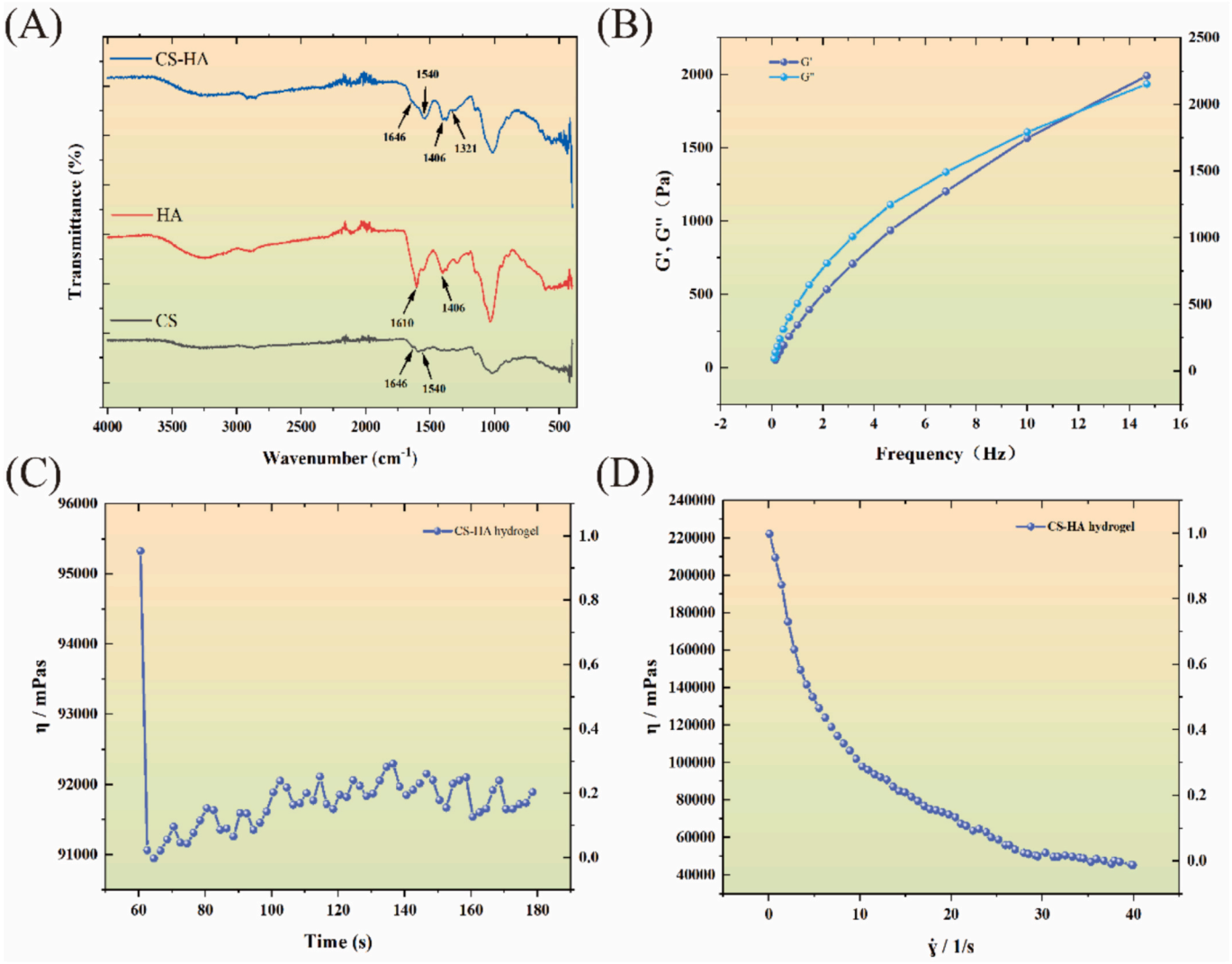

Fig. 3. Rheological and chemical characterization of the chitosan/hyaluronic acid hydrogel (CS-HA hydrogel). (A) Fourier-transform infrared spectroscopy (FTIR) spectra of chitosan, hyaluronic acid and the CS-HA hydrogel. (B) Frequency sweep showing storage modulus (G') and loss modulus (G") of the CS-HA hydrogel. (C) Time-dependent viscosity profile of the CS-HA hydrogel. (D) Shear-rate-dependent viscosity profile of the CS-HA hydrogel.

Chu et al. also indicated that HA and CS bound mainly through physical interactions without forming amide bonds [47].

Subsequently, we tested the rheological properties of the CS-HA hydrogels under different conditions to assess their mechanical behavior (Fig. 3B-D). The higher the vibration frequency of the rheometer, the closer the rheological property of a material is to a solid. The lower the frequency, the closer the material is to a liquid. When the vibration frequency is low, the energy storage modulus G′ and the loss modulus G″ are quite low, indicating liquid-like behavior. If the vibration frequency gradually increases, the energy storage modulus rises and approaches the loss modulus, and the CS-HA hydrogels further forms a reticular structure. When the vibration frequency was higher than 10 Hz, G′ was larger than G″, and the CS-HA hydrogels were a gel state (Fig. 3B). As shown in Fig. 3C, the viscosity scan demonstrated that the viscosity basically remained unchanged with the increase of time. This may be due to the stable crosslinked structure of the hydrogel, and the intermolecular interactions has not change significantly over a short period. The results of the shear viscosity experiment were demonstrated in Fig. 3D. the viscosity of the CS-HA hydrogels were significantly decreased with the increase of shear rate, exhibiting reversible flow behavior within the experimental pressure range. Research indicates that drug delivery systems require carriers capable of maintaining low viscosity to facilitate diffusion while rapidly restoring high viscosity following implantation, thereby prolonging drug retention time [48]. The shear viscosity properties of the CS-HA hydrogels satisfy these drug release requirements, thereby preventing impeded drug release due to excessively high viscosity.

After that, we performed subcutaneous implantation experiments to evaluate the in vivo biocompatibility and preliminary degradation-related histological changes of the CS-HA hydrogels. As shown in Fig. 4, the CS-HA hydrogels did not induce an obvious toxic response in the surrounding skin tissue. On day 7, the implanted CS-HA hydrogels could still be observed under the rat skin, with inflammatory cell infiltration visible around the gel. On day 14, the hydrogel-associated space was markedly reduced, and the skin tissue remained structurally intact with only a few inflammatory cells visible. These findings suggest acceptable local tissue compatibility and preliminary degradation-associated changes. However, because the residual morphology or mass of the hydrogel was not directly quantified at serial time points, Fig. 4 should be interpreted as a histological compatibility observation rather than a full quantitative in vivo degradation evaluation [49].

3.2. *In vivo retention and in vitro release of UCMSCs-exo and biocompatibility analysis of the UCMSCs-exo@CS-HA hydrogels*

Studies have shown that rapid clearance of exosomes in vivo may affect their function, and the retention rate of exosomes after local administration is low. Therefore, the application of exosomes in wound repair remains a major clinical challenge [24]. We used the CS-HA hydrogels as a carrier for UCMSCs-exo. The small-animal imaging

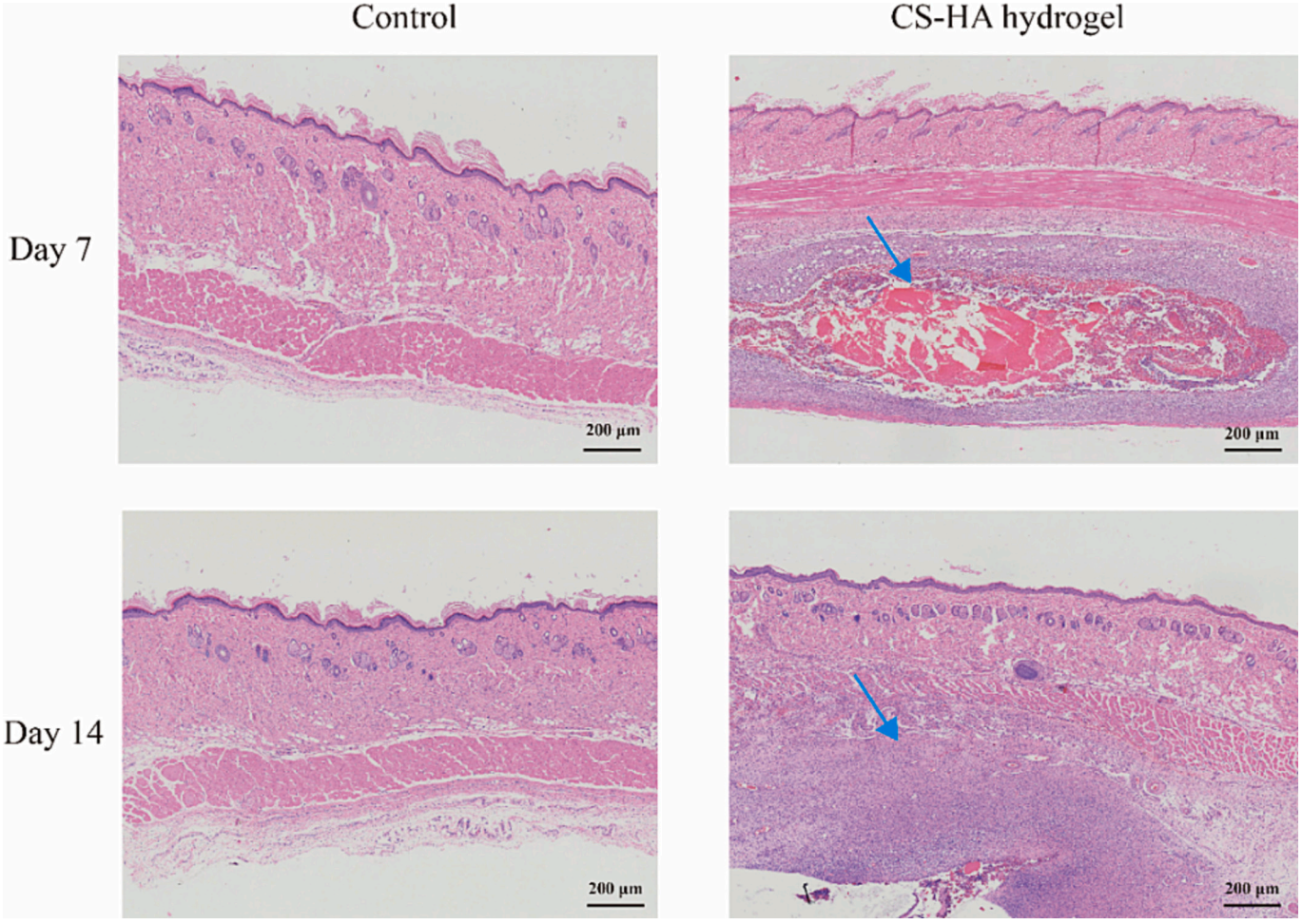

Fig. 4. In vivo biocompatibility and preliminary degradation-associated histological evaluation of the chitosan/hyaluronic acid hydrogel (CS-HA hydrogel) after subcutaneous implantation in rats. Hematoxylin and eosin (H&E)-stained sections show the local tissue response around the implanted hydrogel on days 7 and 14. These images were used to evaluate local tissue compatibility and histological changes associated with hydrogel residue/degradation over time, rather than to provide quantitative degradation kinetics. Scale bars are shown in the corresponding panels.

results shown in Fig. 5A-C demonstrate the in vivo retention of DiR-labeled UCMSCs-exo at the wound site. The UCMSCs-exo@CS-HA hydrogels group exhibited slower fluorescence decay than the free UCMSCs-exo group, and the 3D fluorescence images further indicated improved local retention of UCMSCs-exo. The CS-HA hydrogels may improve UCMSCs-exo retention at the wound site by two mechanisms: (i) UCMSCs-exo can interact with the CS-HA hydrogel network through van der Waals forces, electrostatic attraction, and hydrogen bonding, which improves local utilization; and (ii) the CS-HA hydrogels provide a hydrated extracellular matrix-like microenvironment and a stable carrier for extracellular vesicles [50,51]. As indicated in Fig. 5D, the UCMSCs-exo@CS-HA hydrogels effectively encapsulated UCMSCs-exo and exhibited representative sustained-release behavior in vitro. UCMSCs-exo release reached a peak on the third day and then gradually decreased. This behavior may be attributed to the drug-carrying structure and abundant functional groups of the CS-HA hydrogels, which make them effective carriers for wound dressings [52]. The release kinetics of UCMSCs-exo from the CS-HA hydrogels is a complex process regulated by multiple factors. First, physical encapsulation and diffusion are the dominant mechanisms of initial release. Exosomes are captured in the three-dimensional porous network of hydrogels, and their early release is mainly controlled by Fickian diffusion driven by concentration gradients, with the rate depending on network pore size and connectivity. Second, matrix swelling and degradation dominate subsequent continuous release. Hydrogel swelling in the physiological environment expands the pore size, and endogenous hyaluronidase and lysozyme gradually degrade HA and CS molecular chains over time, causing slow network disintegration and sustained release over several days. Finally, the multi-molecular interactions between the polymer network and the exosome membrane contribute to long-lasting sustained release. Electrostatic adsorption between positively charged chitosan amino groups and the negatively charged exosome membrane, supplemented by hydrophilic and hydrophobic interactions, forms a dynamic capture-release equilibrium, effectively delaying exosome escape. In summary, the sustained-release behavior of UCMSCs-exo@CS-HA is the result of the synergistic effects of physical restriction, matrix degradation, and biomolecular interactions [53].

The biocompatibility of the hydrogel delivery system is also an

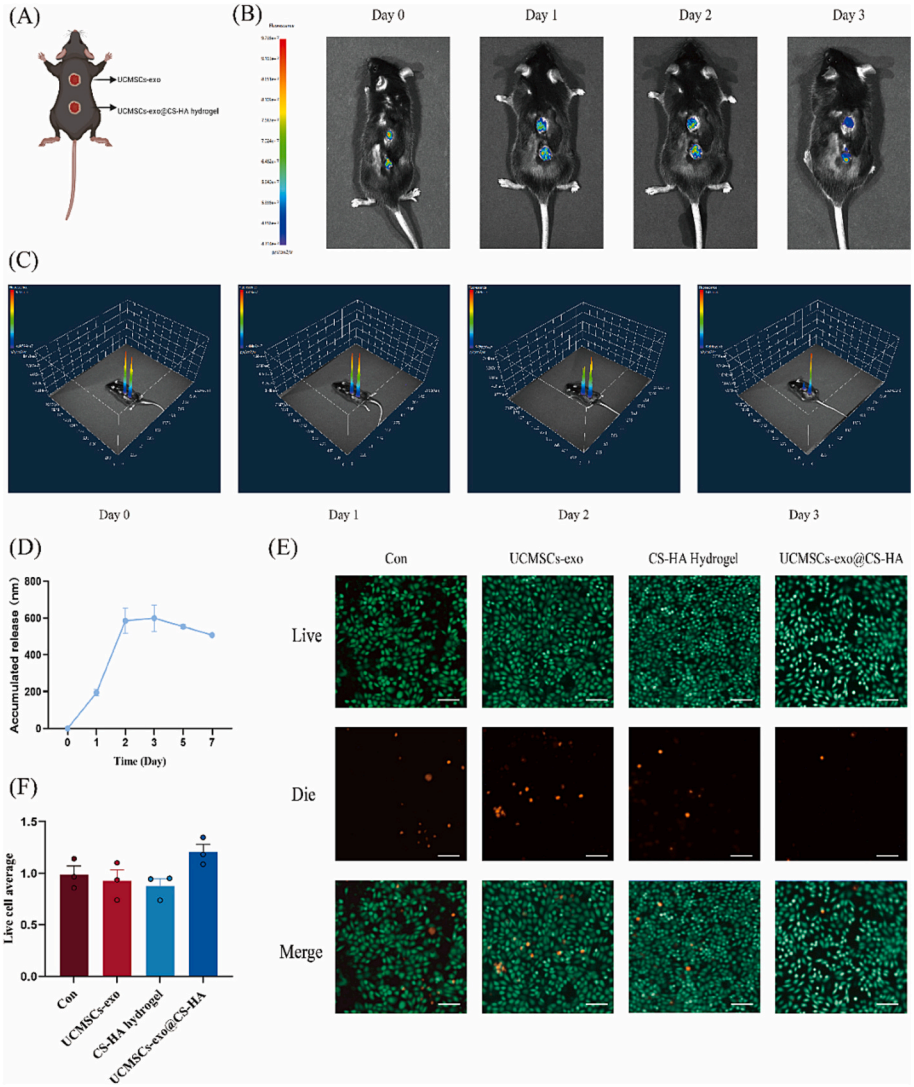

Fig. 5. In vivo retention, in vitro release and biocompatibility evaluation of human umbilical cord mesenchymal stem cell-derived exosome-loaded chitosan/hyaluronic acid hydrogel (UCMSCs-exo@CS-HA). (A-C) Small-animal live fluorescence imaging of DiR-labeled UCMSCs-exo after topical administration of free UCMSCs-exo or UCMSCs-exo@CS-HA hydrogel, showing local exosome retention at the wound site. (D) In vitro cumulative release profile of UCMSCs-exo from the CS-HA hydrogel using a Transwell-based release system. (E) Live/dead staining images of L929 fibroblasts co-cultured with different samples; live cells are shown in green and dead cells in red (original magnification, 200×). (F) Quantitative analysis of live/dead staining. Data are presented as mean +/− standard deviation ($n = 3$) where applicable.

important requirement for wound healing [52]. Most biomaterials used for tissue repair are currently not optimal, mainly because hydrolytic biodegradation processes release acids, which can have toxic effects on cells [54]. Therefore, in the present study, we used live cell staining and CCK8 staining to investigate the cellular biocompatibility of the UCMSCs-exo@CS-HA hydrogels and determine its effects on the proliferation of L929 fibroblasts. The live and dead staining results revealed bright green fluorescence in the fluorescence images of all the experimental groups, but there was little red fluorescence, and there was no significant difference between the groups (Fig. 5E, F).

The CCK8 staining displayed that the effect of the UCMSCs-exo on the proliferation rate of L929 fibroblasts was not significantly different at 24 h. At 48 h, compared with the control group, 2 μg/mL, 5 μg/mL, and 10 μg/mL of the UCMSCs-exo all promoted cell proliferation, with 10 μg/mL of the UCMSCs-exo having the most significant effect ($p < 0.01$). After 72 h, the cell proliferation rate in the 5 μg/mL and 10 μg/mL exosome concentration groups was significantly higher than that in the control group ($p < 0.01$), whereas there was no significant difference in the cell proliferation rate in the 2 μg/mL concentration group (Fig. 6A-C). The reason for promoting fibroblast proliferation may be that the UCMSCs-exo activate intracellular signaling pathways by delivering specific miRNAs or proteins, thus promoting cell proliferation [55,56]. The cytotoxicity results displayed that compared with the control group, the proliferation of L929 fibroblasts was inhibited when the concentration of UCMSCs-exo exceeded 10 μg/mL (Fig. 6D). According to literature reports, when exosomes exceed a certain concentration, their physical and chemical properties may be changed, which will affect their distribution and clearance in organisms, thereby causing toxic reactions [57]. These results indicated that the UCMSCs-exo@CS-HA hydrogels had good biocompatibility and proliferation ability of L929 fibroblasts. After that, we further investigated the ability of the UCMSCs-exo@CS-HA hydrogels to promote the proliferation and migration of L929 fibroblasts through scratch experiments. As illuminated in Fig. 6E-F, compared with the control group, the UCMSCs-exo@CS-HA hydrogels significantly promoted the proliferation and migration of L929 fibroblasts after 24 h. This can be attributed to the fact that the CS-HA hydrogels contain several motifs that can interact with cellular instructor receptors, which provide an excellent growth scaffold for cell growth [13]. In addition, UCMSCs-exo may deliver bioactive RNA/protein cargo and activate intracellular signaling pathways that support cell proliferation and migration [32,55].

3.3. Antibacterial activity of the UCMSCs-exo@CS-HA hydrogels

Bacterial contamination is an important risk factor that may delay wound repair and aggravate inflammation [52,58,59]. *Escherichia coli* can be associated with local tissue infection under certain conditions [26], whereas *Staphylococcus aureus* is one of the most common pathogens related to skin and soft-tissue infections [60–62]. In recent years, mesenchymal stem cell-derived exosomes and porous hydrogel dressings have been reported to exhibit antibacterial or bacteria-limiting effects [63]. In this study, the inhibitory effects of UCMSCs-exo@CS-HA hydrogels against *S. aureus* and *E. coli* were evaluated by in vitro antibacterial experiments. As shown in Fig. 7A, treatment with UCMSCs-exo@CS-HA hydrogels reduced the number of visible colonies of both *E. coli* and *S. aureus* after 24 h. As displayed in Fig. 7B, the inhibitory ability against *E. coli* increased in the order of CS-HA hydrogels, UCMSCs-exo, and UCMSCs-exo@CS-HA hydrogels, and the antibacterial rate of the UCMSCs-exo@CS-HA hydrogels group reached 93% ± 3% ($p < 0.01$). As shown in Fig. 7C, antibacterial activity against *S. aureus* was also enhanced in the UCMSCs-exo@CS-HA hydrogels group compared with the control group ($p < 0.01$). This effect may be related to the positively charged amino groups of CS under weakly acidic conditions, which can interact with negatively charged bacterial surfaces, increase membrane permeability, and disrupt bacterial growth [64,65]. In addition, UCMSCs-exo may contribute antibacterial components or immunomodulatory bioactive cargo, thereby cooperating with the CS-HA matrix [66]. Importantly, the present animal study used an aseptic acute full-thickness wound model and did not include standardized bacterial inoculation. Therefore, wound-site colony-forming unit quantification would not provide a valid assessment of antibacterial efficacy in this model. Accordingly, the antibacterial conclusion of this study is restricted to the in vitro bacterial assays, and in vivo antibacterial performance should be further examined in an infected wound model.

3.4. The UCMSCs-exo@CS-HA hydrogels promoted wound healing in mice

Wound healing is an important and complex process, and its effectiveness is mainly reflected in the regeneration of abundant hair follicles, the formation of new capillaries, the orderly deposition of collagen, the disappearance of inflammatory exudates, and re-epithelialization [67]. To investigate the effect of UCMSCs-exo@CS-HA hydrogels on wound healing, we established a complete model of wound defects in mice. The results of wound healing in mice were shown in Fig. 8A -B. All the experimental groups exhibited a reduction in wound area by Day 10, and the UCMSCs-exo@CS-HA group had the best healing rate of 98%. This was followed by the CS-HA hydrogels group, the UCMSCs-exo group, and the control group. The pathological manifestations of wound healing were then assessed by HE staining. The results in Fig. 8C displayed that on Day 10 of wound repair, the inflammatory response was reduced in the UCMSCs-exo group compared with the control group. Neoplastic hair follicle tissue and re-epithelialization of the wound tissue were present in the CS-HA hydrogels group compared with the UCMSCs-exo group. Compared with the wound tissues in the CS-HA hydrogels group, the wound tissues in the UCMSCs-exo@CS-HA hydrogels group were less inflamed, contained a large amount of neoplastic hair follicles and neovascular tissues, and were structurally similar to normal tissues. The UCMSCs-exo@CS-HA hydrogel's promotion of wound healing in mice can be attributed to the UCMSCs-exo can induce the production of growth factors that promote fibroblast growth [68]. Meanwhile, CS absorbs and retains water, providing a moist healing environment for the wound [44]. HA is a major component of the skin's extracellular matrix and is involved in angiogenesis, and promoting tissue regeneration [69]. Due to the synergistic effect of CS and HA, the CS-HA hydrogels has anti-inflammatory, and antibacterial properties, thus promoting wound healing.

3.5. The UCMSCs-exo@CS-HA promoted wound collagen deposition and angiogenesis

Proper collagen deposition improves wound healing. Collagen is a core component of the extracellular matrix and is an important signaling molecule in the wound-healing process [70]. In the study, we investigated collagen deposition in each experimental group on the tenth day of wound healing by Masson staining. The ability to promote collagen fiber proliferation compared to the control group was in the order of the UCMSCs-exo@CS-HA group, the CS-HA hydrogels group, and the UCMSCs-exo group ($p < 0.01$). The visible amount of collagen fibers increased successively, the arrangement of collagen fibers was gradually orderly, and Masson staining changed from light blue to dark blue (Fig. 9A, C). We believe that UCMSCs-exo@CS-HA promotes collagen deposition not through a single pathway, but rather as a result of the synergistic effect of its unique “sustained-release delivery” and “multifunctional exosome” properties. Firstly, the sustained-release property of hydrogels ensures a continuous supply of exosomes, enabling them to act on fibroblasts, the key cells for wound repair, for a long time and providing a continuous signal for their proliferation and activation. UCMSCs-exo is rich in various active factors, such as miR-21-5p and growth factors TGF-β and FGF [32], which can be continuously and controllably released into wound microenvironment by CS-HA hydrogels. After being taken up by the surrounding fibroblasts, these factors

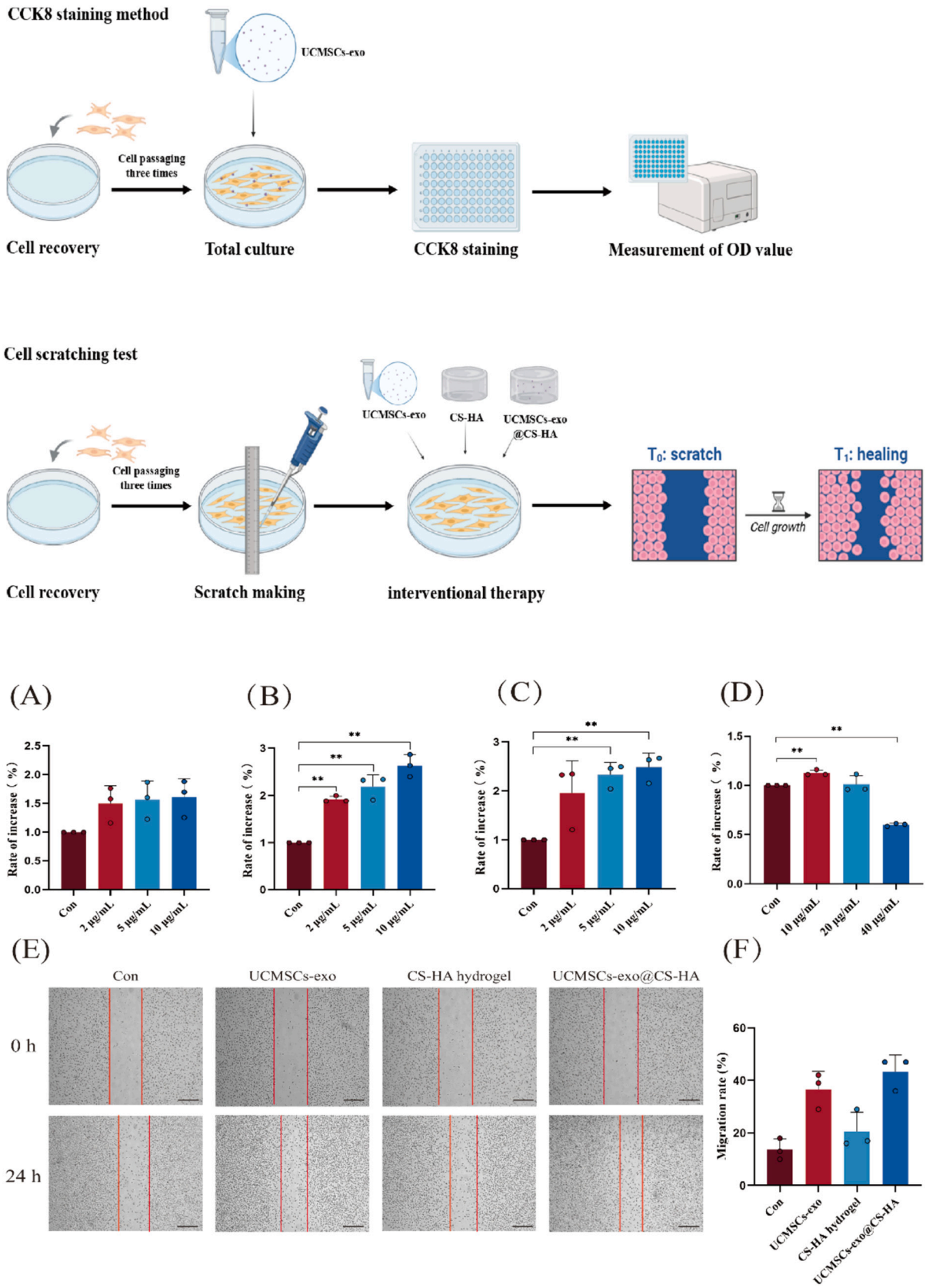

Fig. 6. Cell proliferation, cytotoxicity and scratch-wound migration assays. (A-C) Cell Counting Kit-8 (CCK-8) assay evaluating the effect of different concentrations of human umbilical cord mesenchymal stem cell-derived exosomes (UCMSCs-exo) on L929 fibroblast proliferation at 24, 48 and 72 h (n = 3). (D) Quantitative cytotoxicity analysis of UCMSCs-exo at different concentrations (n = 3). (E, F) Representative images and quantitative analysis of L929 fibroblast migration in the scratch-wound assay (original magnification, 400×). Data are presented as mean +/− standard deviation. Differences between groups were analyzed using one-way analysis of variance (ANOVA) followed by multiple-comparison testing; *$p < 0.05$ and **$p < 0.01$ indicate statistically significant differences.

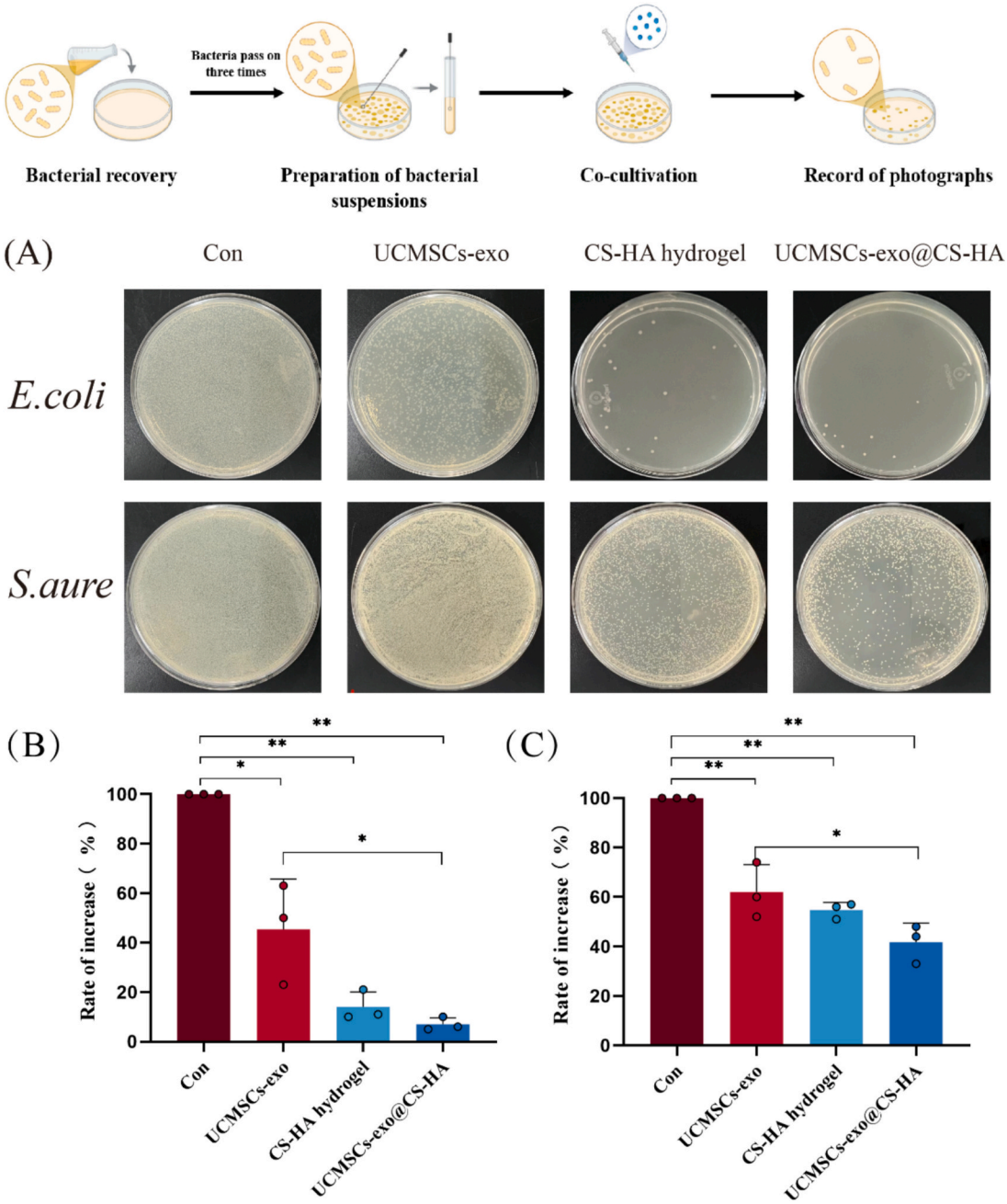

Fig. 7. In vitro antibacterial activity of human umbilical cord mesenchymal stem cell-derived exosome-loaded chitosan/hyaluronic acid hydrogel (UCMSCs-exo@CS-HA). (A) Representative bacterial colony images showing antibacterial effects against *Escherichia coli* (*E. coli*) ATCC 25922 and *Staphylococcus aureus* (*S. aureus*) ATCC 25923 after 24 h incubation. (B) Quantitative antibacterial rate against *E. coli* (n = 3). (C) Quantitative antibacterial rate against *S. aureus* (n = 3). Data are presented as mean +/− standard deviation. Differences between groups were analyzed using one-way analysis of variance (ANOVA) followed by multiple-comparison testing; $*p < 0.05$ and $**p < 0.01$ indicate statistically significant differences.

can promote the proliferation and activation of fibroblasts and upregulate their key ability to synthesize collagen. Furthermore, CS-HA hydrogels promote collagen synthesis by indirectly regulating the wound microenvironment.

According to the literature, in the stage of wound healing and proliferation, the density of new capillaries is 2–3 or even 10 times higher than that of normal tissue. In contrast, in the later stages of wound healing, the new capillaries gradually close and resemble the structure of normal skin tissue [2,71]. Blood vessels are crucial for tissue regeneration and wound repair because they provide nutrients and oxygen to the cells around the wound. In our experiments, angiogenesis in wound tissue was analyzed using immunohistochemical methods. As proved in the resultant graphs (Fig. 9B, D-F), compared with the control group, the positive expression of CD31 in the UCMSCs-exo and CS-HA hydrogels groups was increased, and the number of neovascularization was increased. In contrast, the UCMSCs-exo@CS-HA hydrogels group exhibited vascular closure, almost complete wound healing compared with the control, the UCMSCs-exo and the CS-HA hydrogels group ($p < 0.05$). Furthermore, compared with the control group, UCMSCs-exo and CS-HA hydrogels groups, the expression of VEGF in the UCMSCs-exo@CS-HA hydrogels group was significantly increased ($p < 0.01$). The decrease of VEGF secretion is considered to lead to the damage of tissue repair, which is the key molecular target of angiogenesis in the treatment of regenerative skin [72]. Compared with the control group,

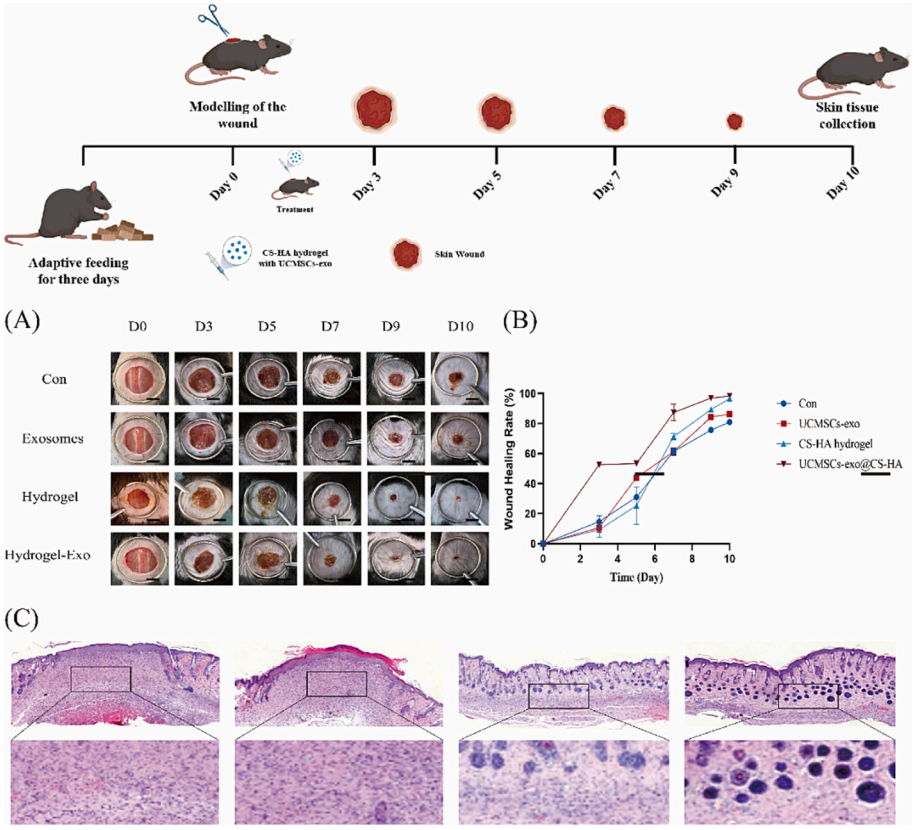

Fig. 8. Evaluation of wound closure and histological repair in the mouse full-thickness skin wound model. (A) Representative wound images at different time points after treatment with control, chitosan/hyaluronic acid hydrogel (CS-HA hydrogel), human umbilical cord mesenchymal stem cell-derived exosomes (UCMSCs-exo), or UCMSCs-exo@CS-HA hydrogel ($n = 6$ for wound-area quantification). (B) Quantitative analysis of wound closure rate. (C) Hematoxylin and eosin (H&E) staining of wound tissues on day 10, scale bar = 500 μm. Data are presented as mean +/− standard deviation where applicable.

UCMSCs-exo and CS-HA hydrogels groups, the expression of HIF-1α in the UCMSCs-exo@CS-HA hydrogels group was also increased. HIF-1α is one of the most important indicators of wound angiogenesis and is a key regulator of wound re-epithelialization and angiogenesis [73]. The pro-angiogenic capability of the UCMSCs-exo@CS-HA hydrogels may be attributed to the ability of CS and HA to increase the expression levels of peri-wound repair factors and apoptotic factors to promote angiogenesis, epidermal regeneration, and cell proliferation [13]. It is also due to the ability of the UCMSCs-exo to enhance the angiogenic activity of endothelial cells [22,74].

3.6. *The UCMSCs-exo@CS-HA hydrogels reduced the expression of inflammatory factors and promoted wound healing*

In the present study, the anti-inflammatory capability of the UCMSCs-exo@CS-HA hydrogels and its ability to promote collagen fiber proliferation was further confirmed by western blot analysis (Fig. 10A-E). Studies have revealed that collagen I predominates during the later stages of wound healing, and its significant deposition may lead to scarring. In contrast to collagen I, the increase in collagen III helps reduce the development of wound scars [75]. The quantitative data of western blotting images showed that compared with the control group, the CS-HA hydrogels group and the UCMSCs-exo group, the expression of collagen I in the UCMSCs-exo@CS-HA hydrogels group was significantly decreased ($p < 0.05$) (Fig. 10B). The results were shown in Fig. 10C, compared with the control group, the expression of collagen III was evidently increased in the UCMSCs-exo@CS-HA hydrogels group ($p < 0.05$). Compared with the CS-HA hydrogels and UCMSCs-exo hydrogels groups, the expression of collagen III was also increased in the UCMSCs-exo@CS-HA hydrogels group. Studies have exhibited that COX2 and iNOS are common inflammatory factors in wound healing. The research of Li et al. also obtained the same result [19].

Additionally, excessive inflammation can lead to impaired wound healing [76]. As shown in Fig. 10D, compared with the control group, the CS-HA hydrogels group and the UCMSCs-exo group, COX2 expression was significantly inhibited in the UCMSCs-exo@CS-HA group ($p < 0.01$). Furthermore, as shown in Fig. 10E, the expression of iNOS was reduced in the UCMSCs-exo@CS-HA hydrogels group compared with the control group ($p < 0.05$), and it was also lower than that in the CS-HA hydrogels and UCMSCs-exo groups. These results support that UCMSCs-exo@CS-HA hydrogels attenuated inflammatory-factor expression in wound tissue. This effect may be attributed to the capacity of UCMSCs-exo to deliver RNAs, proteins, and cytokine-related cargo with anti-inflammatory activity [77], as well as to the local retention provided by the CS-HA hydrogel network [22]. Nevertheless, because the western blot assay was performed using whole wound tissue, iNOS expression in this study should be interpreted as a tissue-level inflammatory indicator rather than a macrophage-specific M1 marker. We did not directly detect macrophage polarization markers, such as CD86/iNOS for the M1 phenotype or CD206/Arg-1 for the M2 phenotype, by immunofluorescence, flow cytometry, or double immunostaining. Therefore, we have avoided claiming direct regulation of macrophage polarization and have limited the conclusion to inflammatory-factor modulation. The potential effect of UCMSCs-exo@CS-HA hydrogels on macrophage phenotype switching will be investigated in future work. These evidence boundaries were considered when interpreting the biological effects of the hydrogel, and the proposed anti-inflammatory role should therefore be understood as wound-tissue inflammatory-factor attenuation rather than direct proof of macrophage reprogramming.

Several limitations should be acknowledged. First, the antibacterial

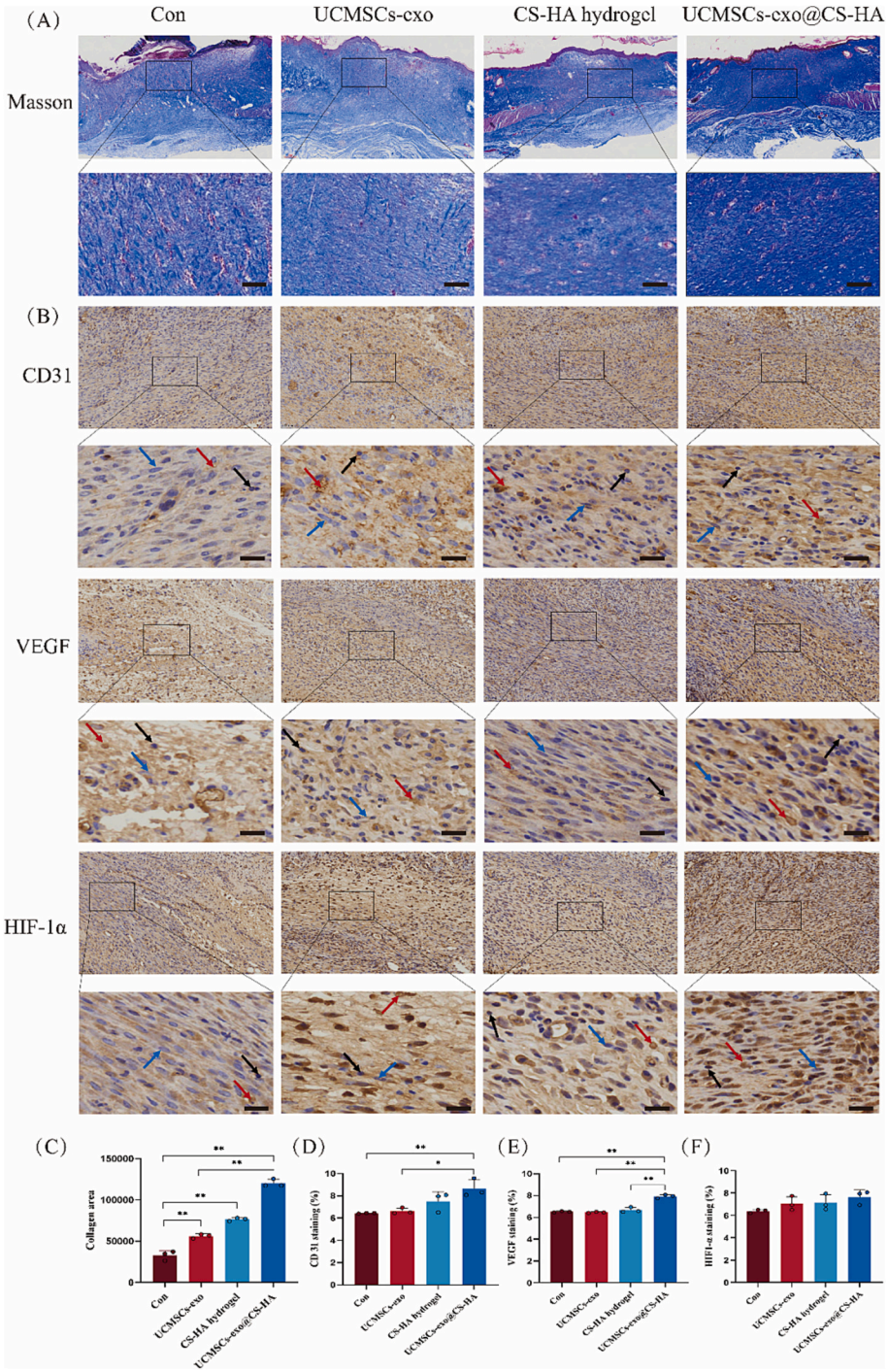

Fig. 9. Masson staining and immunohistochemical analysis of collagen deposition and angiogenesis in wound tissues on day 10. (A, C) Representative Masson staining images and quantitative analysis of collagen deposition, scale bar = 300 μm. (B) Representative immunohistochemical staining images; red arrows indicate blood vessels, blue arrows indicate fibroblasts and black arrows indicate macrophage-like inflammatory cells, scale bar = 50 μm. (D-F) Quantitative analysis of vascular-related markers, including cluster of differentiation 31 (CD31), vascular endothelial growth factor (VEGF) and hypoxia-inducible factor 1 alpha (HIF-1alpha). Data are presented as mean +/− standard deviation. Differences between groups were analyzed using one-way analysis of variance (ANOVA) followed by multiple-comparison testing; *$p < 0.05$ and **$p < 0.01$ indicate statistically significant differences.

effect was verified by in vitro colony assays, whereas the in vivo wound model was an aseptic acute full-thickness defect model rather than an infected wound model; therefore, in vivo antibacterial efficacy requires further validation using standardized bacterial inoculation and wound-site colony-forming unit quantification. Second, inflammatory regulation was evaluated by whole-tissue COX2 and iNOS expression, and macrophage polarization was not directly examined using macrophage-specific double staining, flow cytometry, or phenotype markers. Third, the histological implantation assay provides preliminary degradation-related and compatibility evidence, but direct residual hydrogel morphology or mass-loss tracking over time was not performed. These limitations have been considered when drawing the conclusions of this study.

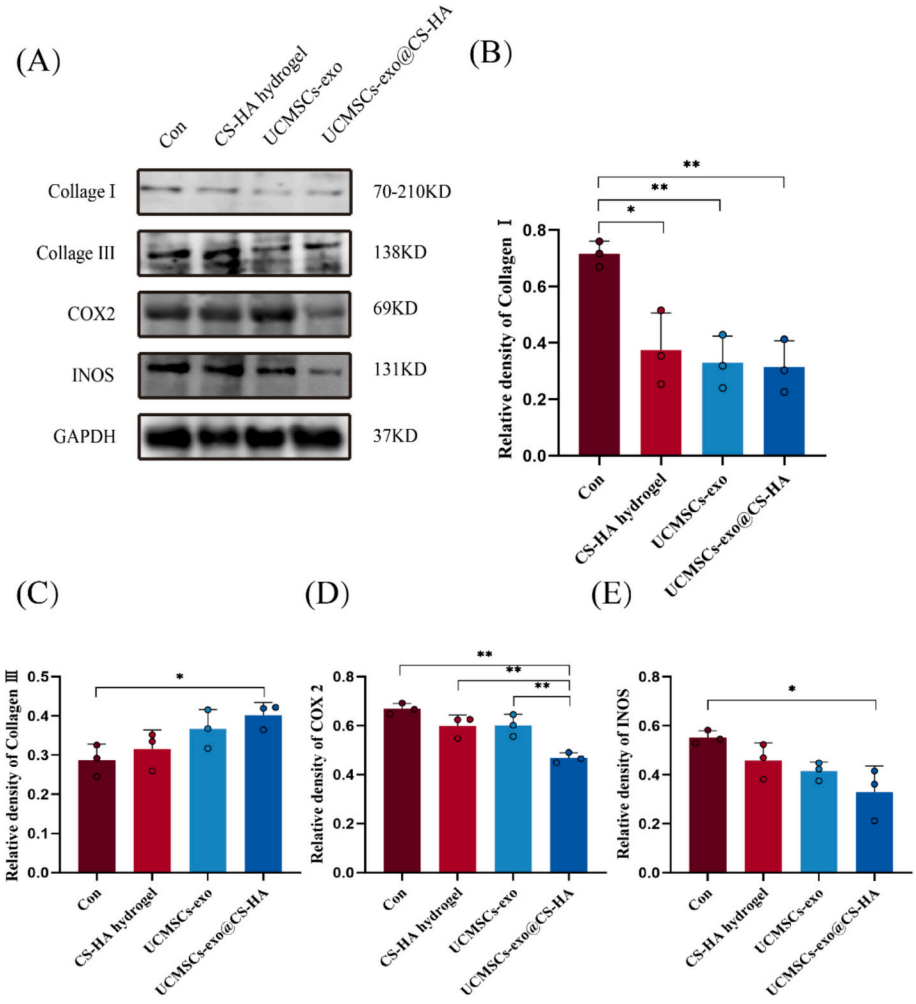

Fig. 10. Western blot analysis of collagen remodeling- and inflammation-related proteins in wound tissues. (A) Representative western blot bands for collagen I, collagen III, cyclooxygenase-2 (COX-2) and inducible nitric oxide synthase (iNOS). (B-E) Quantitative analysis of protein expression levels normalized to the corresponding loading control (n = 3). Data are presented as mean +/− standard deviation. Differences between groups were analyzed using one-way analysis of variance (ANOVA) followed by multiple-comparison testing; *$p < 0.05$ and **$p < 0.01$ indicate statistically significant differences.

4. Conclusions

In this study, the CS-HA hydrogels were prepared by a physical crosslinking method, and their physicochemical and biological properties were analyzed. The results suggested that the CS-HA hydrogels had excellent rheological and biological properties and could provide a suitable environment for the storage and sustained release of extracellular vesicles. Then, 10 μg/mL UCMSCs-exo was added to the CS-HA hydrogels to obtain the UCMSCs-exo@CS-HA hydrogels delivery system. The in vitro antibacterial experiment and cell experiment demonstrated that the gel could inhibit the proliferation of *E. coli* and *S. aureus* and promote the proliferation and migration of L929 fibroblasts. In addition, in vivo imaging and in vitro release experiments suggested that the CS-HA hydrogels could enhance the local retention and sustained release of UCMSCs-exo. Animal experiments suggested that UCMSCs-exo@CS-HA hydrogels could promote acute skin wound healing, regulate collagen expression, and accelerate wound re-epithelialization and neovascularization. Moreover, the UCMSCs-exo@CS-HA hydrogels inhibited the expression of inflammatory factors COX2 and iNOS and regulated the expression of wound collagen I and collagen III. It should be emphasized that the current in vivo model was an aseptic acute wound model; therefore, in vivo antibacterial efficacy was not assessed by wound-site CFU counting. In addition, macrophage polarization was not directly verified using macrophage-specific markers. These points represent important directions for future infected wound and immunophenotyping studies. In summary, the prepared UCMSCs-exo@CS-HA hydrogels provide a promising method for the treatment of acute skin injury. Within the limits of the current experimental design, these findings support UCMSCs-exo@CS-HA hydrogels as a promising polysaccharide-based exosome delivery dressing for acute skin repair, while infected-wound antibacterial efficacy and macrophage phenotype regulation require further dedicated studies.

CRediT authorship contribution statement

Zhonghua Luo: Writing – original draft, Visualization, Methodology, Funding acquisition. **Zhiquan Hou:** Writing – original draft, Methodology, Funding acquisition, Formal analysis. **Mi Wu:** Methodology, Investigation, Data curation. **Yan Zhao:** Supervision, Formal analysis. **Fuhai Hui:** Data curation, Conceptualization. **Yudong Wu:** Resources. **Yuan Wang:** Writing – review & editing, Project administration. **Yunen Liu:** Writing – review & editing, Project administration.

Ethical statement

All procedures followed the guidelines for the care and use of laboratory animals and the ethical criteria outlined by the National Scientific Research Council.

Funding

This study was supported by the Shenyang Natural Science Foundation Special Project (23-503-6-14), the Joint Program of Science and Technology Plans of Liaoning Province (2024011888-JH3/4700) and (No. Y20240511).

Declaration of competing interest

The authors declare that they have no known competing financial interests or personal relationships that could have appeared to influence the work reported in this paper.

Data availability

The authors do not have permission to share data.

References

[1] H. Jo, S. Brito, B.M. Kwak, S. Park, M.G. Lee, B.H. Bin, Applications of mesenchymal stem cells in skin regeneration and rejuvenation, Int. J. Mol. Sci. 22 (5) (2021) 2410.
[2] M. Rodrigues, N. Kosaric, C.A. Bonham, G.C. Gurtner, Wound healing: a cellular perspective, Physiol. Rev. 99 (1) (2019) 665–706.
[3] T. Jiang, Q. Li, J. Qiu, J. Chen, S. Du, X. Xu, Z. Wu, X. Yang, Z. Chen, T. Chen, Nanobiotechnology: applications in chronic wound healing, Int. J. Nanomedicine 17 (2022) 3125–3145.
[4] T. Guan, J. Li, C. Chen, Y. Liu, Self-assembling peptide-based hydrogels for wound tissue repair, Adv Sci (Weinh). 9 (10) (2022) e2104165.
[5] R. Dimatteo, N.J. Darling, T. Segura, In situ forming injectable hydrogels for drug delivery and wound repair, Adv. Drug Deliv. Rev. 127 (2018) 167–184.
[6] W. Li, Q. Chen, Y. Ma, H. Su, H. Ren, H. Wang, Antibacterial hydrogels for bacteria-infected wound treatment, Biomed. Tech. 9 (2025) 100066, https://doi.org/10.1016/j.bmt.2024.11.001.
[7] Z. Tang, Q. Xia, J. Li, J. Chen, X. Wu, J. Li, J. Liu, W. Liu, K. Rong, X. Meng, Microenvironment-feedback hydrogel for precise sequential repair of acute infectious wounds, Biomed. Tech. 12 (2025) 100120, https://doi.org/10.1016/j.bmt.2025.100120.
[8] X. Xue, Y. Hu, S. Wang, X. Chen, Y. Jiang, J. Su, Fabrication of physical and chemical crosslinked hydrogels for bone tissue engineering, Bioact. Mater. 12 (2022) 327–339.
[9] S. Alven, B.A. Aderibigbe, Chitosan and cellulose-based hydrogels for wound management, Int. J. Mol. Sci. 21 (24) (2020) 9656.
[10] L. Pourtalebi Jahromi, M. Rothammer, G. Fuhrmann, Polysaccharide hydrogel platforms as suitable carriers of liposomes and extracellular vesicles for dermal applications, Adv. Drug Deliv. Rev. 200 (2023) 115028.
[11] H. Ababneh, B.H. Hameed, Chitosan-derived hydrothermally carbonized materials and its applications: a review of recent literature, Int. J. Biol. Macromol. 186 (2021) 314–327.
[12] J. Maitz, J. Merlino, S. Rizzo, G. McKew, P. Maitz, Burn wound infections microbiome and novel approaches using therapeutic microorganisms in burn wound infection control, Adv. Drug Deliv. Rev. 196 (2023) 114769.
[13] M.A. Matica, F.L. Aachmann, A. Tøndervik, H. Sletta, V. Ostafe, Chitosan as a wound dressing starting material: antimicrobial properties and mode of action, Int. J. Mol. Sci. 20 (23) (2019) 5889.
[14] K. Mohan, A.R. Ganesan, T. Muralisankar, R. Jayakumar, P. Sathishkumar, V. Uthayakumar, R. Chandirasekar, N. Revathi, Recent insights into the extraction, characterization, and bioactivities of chitin and chitosan from insects, Trends Food Sci. Technol. 105 (2020) 17–42.
[15] L. Ding, Y. Li, Y. Yang, S. Song, H. Qi, J. Wang, Z. Wang, J. Zhao, W. Zhang, L. Zhao, D. Zhao, X. Li, Z. Wang, Wenfei Buqi Tongluo formula against bleomycin-induced pulmonary fibrosis by inhibiting TGF-β/Smad3 pathway, Front. Pharmacol. 12 (2022) 762998.
[16] J.A. Burdick, G.D. Prestwich, Hyaluronic acid hydrogels for biomedical applications, Adv. Mater. 23 (12) (2011) H41–H56.
[17] A. Yasin, Y. Ren, J. Li, Y. Sheng, C. Cao, K. Zhang, Advances in hyaluronic acid for biomedical applications, Front. Bioeng. Biotechnol. 10 (2022) 910290.
[18] G. Abatangelo, V. Vindigni, G. Avruscio, L. Pandis, P. Brun, Hyaluronic acid: redefining its role, Cells 9 (7) (2020) 1743.
[19] J. Li, J. Su, J. Liang, K. Zhang, M. Xie, B. Cai, J. Li, A hyaluronic acid/chitosan composite functionalized hydrogel based on enzyme-catalyzed and Schiff base reaction for promoting wound healing, Int. J. Biol. Macromol. 255 (2024) 128284.
[20] A. Sobhani, N. Khanlarkhani, M. Baazm, F. Mohammadzadeh, A. Najafi, S. Mehdinejadiani, F. Sargolzaei Aval, Multipotent stem cell and current application, Acta Med Iran. 55 (1) (2017) 6–23.
[21] L. Lu, Y.J. Liu, S.G. Yang, Q.J. Zhao, X. Wang, W. Gong, Z.B. Han, Z.S. Xu, Y.X. Lu, D. Liu, Z.Z. Chen, Z.C. Han, Isolation and characterization of human umbilical cord mesenchymal stem cells with hematopoiesis-supportive function and other potentials, Haematologica 91 (8) (2006) 1017–1026.
[22] X. Zhao, L. Fu, H. Zou, Y. He, Y. Pan, L. Ye, Y. Huang, W. Fan, J. Zhang, Y. Ma, J. Chen, M. Zhu, C. Zhang, Y. Cai, X. Mou, Optogenetic engineered umbilical cord MSC-derived exosomes for remodeling of the immune microenvironment in diabetic wounds and the promotion of tissue repair, J Nanobiotechnology. 21 (1) (2023) 176.
[23] N.B. Vu, H.T. Nguyen, R. Palumbo, R. Pellicano, S. Fagoonee, P.V. Pham, Stem cell-derived exosomes for wound healing: current status and promising directions, Minerva Med. 112 (3) (2021) 384–400.
[24] C. Wang, M. Wang, T. Xu, X. Zhang, C. Lin, W. Gao, C. Mao, Engineering bioactive self-healing antibacterial exosomes hydrogel for promoting chronic diabetic wound healing and complete skin regeneration, Theranostics 9 (1) (2019) 65–76.
[25] Y. Song, Y. You, X. Xu, J. Lu, X. Huang, J. Zhang, Y. Du, Adipose-derived mesenchymal stem cell-derived exosomes biopotentiated extracellular matrix hydrogels accelerate diabetic wound healing and skin regeneration, Adv. Sci. (Weinh). 10 (30) (2023) e2304023.
[26] Y. Ju, Y. Hu, P. Yang, X. Xie, B. Fang, Extracellular vesicle-loaded hydrogels for tissue repair and regeneration, Mater Today Bio 18 (2022) 100522.
[27] R. Shi, Y. Jin, W. Hu, W. Lian, C. Cao, S. Han, H. Zhao, Exosomes derived from mmu_circ_0000250-modified adipose-derived mesenchymal stem cells promote wound healing in diabetic mice by inducing miR-128-3p/SIRT1-mediated autophagy, Am. J. Physiol. Cell Physiol. 318 (5) (2020) C848–c856.
[28] A. Charrier, R. Chen, L. Chen, S. Kemper, T. Hattori, M. Takigawa, D.R. Brigstock, Exosomes mediate intercellular transfer of pro-fibrogenic connective tissue growth factor (CCN2) between hepatic stellate cells, the principal fibrotic cells in the liver, Surgery 156 (3) (2014) 548–555.
[29] M. Wu, D. Deng, D. Peng, C. Tan, J. Lv, W. Zhang, Y. Zhao, Development of low-molecular-weight polysaccharide-based wound dressings for full-thickness cutaneous wound healing via coacervate formation, Carbohydr. Polym. 348 (Pt A) (2025) 122851.
[30] N. Narayanan, Z. Jia, K.H. Kim, L. Kuang, P. Lengemann, G. Shafer, M. Deng, Biomimetic glycosaminoglycan-based scaffolds improve skeletal muscle regeneration in a murine volumetric muscle loss model, Bioact. Mater. 6 (4) (2021) 1201–1213.
[31] H. Li, X. Wei, X. Yi, S. Tang, J. He, Y. Huang, F. Cheng, Antibacterial, hemostasis, adhesive, self-healing polysaccharides-based composite hydrogel wound dressing for the prevention and treatment of postoperative adhesion, Mater. Sci. Eng. C Mater. Biol. Appl. 123 (2021) 111978.
[32] J. Wang, K. Chen, Y. Chen, M. Li, S. Li, T. Wen, H. Wang, S. Zhao, L. Chen, Y. Zhao, Exosomes derived from mesenchymal stem cells: the role in tissue repair, Bioact. Mater. 28 (2023) 170–205.
[33] P. Guan, C. Liu, D. Xie, S. Mao, Y. Ji, Y. Lin, Y. Sun, Exosome-loaded extracellular matrix-mimic hydrogel with anti-inflammatory property facilitates/promotes growth plate injury repair, Bioact. Mater. 10 (2022) 145–158.
[34] W. Sun, Z. Li, X. Zhou, G. Yang, L. Yuan, Efficient exosome delivery in refractory tissues assisted by ultrasound-targeted microbubble destruction, Drug Deliv. 26 (1) (2019) 45–50.
[35] Z. Chen, L. Wang, C. Guo, M. Qiu, L. Cheng, K. Chen, Y. Yan, Vascularized polypeptide hydrogel modulates macrophage polarization for wound healing, Acta Biomater. 155 (2023) 218–234.
[36] Y. Wang, Y. Zan, Y. Huang, X. Peng, S. Ma, J. Ren, Y. Ding, NSUN2 alleviates doxorubicin-induced myocardial injury through Nrf2-mediated antioxidant stress, Cell Death Discov. 9 (1) (2023) 43.
[37] L. Qian, L. Pi, B.R. Fang, X.X. Meng, Adipose mesenchymal stem cell-derived exosomes accelerate skin wound healing via the lncRNA H19/miR-19b/SOX9 axis, Lab. Invest. 101 (9) (2021) 1254–1266.
[38] L. Zhang, W. Niu, Y. Lin, J. Ma, T. Leng, W. Cheng, B. Lei, Multifunctional antibacterial bioactive nanoglass hydrogel for normal and MRSA infected wound repair, J Nanobiotechnology. 21 (1) (2023) 162.
[39] T.Y. Chen, T.K. Wen, N.T. Dai, S.H. Hsu, Cryogel/hydrogel biomaterials and acupuncture combined to promote diabetic skin wound healing through immunomodulation, Biomaterials 269 (2021) 120608.
[40] Y. Chen, X. Zhang, Z. Liu, J. Yang, C. Chen, J. Wang, W. He, Obstruction of the formation of granulation tissue leads to delayed wound healing after scald burn injury in mice, Burns Trauma 9 (2021) tkab004.
[41] S. Liu, N. Jiang, Y. Chi, Q. Peng, G. Dai, L. Qian, W. Yue, Injectable and self-healing hydrogel based on chitosan-tannic acid and oxidized hyaluronic acid for wound healing, ACS Biomater Sci. Eng. 8 (9) (2022) 3754–3764.
[42] W. Zhu, Y. Dong, P. Xu, Q. Pan, K. Jia, P. Jin, B. Cheng, A composite hydrogel containing resveratrol-laden nanoparticles and platelet-derived extracellular vesicles promotes wound healing in diabetic mice, Acta Biomater. 154 (2022) 212–230.
[43] D.R. Griffin, M.M. Archang, C.H. Kuan, W.M. Weaver, J.S. Weinstein, A.C. Feng, P. O. Scumpia, Activating an adaptive immune response from a hydrogel scaffold imparts regenerative wound healing, Nat. Mater. 20 (4) (2021) 560–569.
[44] W. Feng, Z. Wang, Shear-thinning and self-healing chitosan-graphene oxide hydrogel for hemostasis and wound healing, Carbohydr. Polym. 294 (2022) 119824.
[45] W. Chen, N. Li, Y. Ma, M.L. Minus, K. Benson, X. Lu, H. Zhu, Superstrong and tough hydrogel through physical cross-linking and molecular alignment, Biomacromolecules 20 (12) (2019) 4476–4484.
[46] J. Li, F. Yu, G. Chen, J. Liu, X.L. Li, B. Cheng, J.F. Pan, Moist-retaining, self-recoverable, bioadhesive, and transparent in situ forming hydrogels to accelerate wound healing, ACS Appl. Mater. Interfaces 12 (2) (2020) 2023–2038.
[47] W. Chu, P. Wang, Z. Ma, L. Peng, C. Guo, Y. Fu, L. Ding, Lupeol-loaded chitosan-Ag (+) nanoparticle/sericin hydrogel accelerates wound healing and effectively inhibits bacterial infection, Int. J. Biol. Macromol. 243 (2023) 125310.

[48] G. Stojkov, Z. Niyazov, F. Picchioni, R.K. Bose, Relationship between structure and rheology of hydrogels for various applications, Gels 7 (4) (2021) 255.
[49] A.M. Hawkins, T.A. Milbrandt, D.A. Puleo, J.Z. Hilt, Composite hydrogel scaffolds with controlled pore opening via biodegradable hydrogel porogen degradation, J. Biomed. Mater. Res. A 102 (2) (2014) 400–412.
[50] O.P. Wiklander, J.Z. Nordin, A. O'Loughlin, Y. Gustafsson, G. Corso, I. Mäger, S. E. Andaloussi, Extracellular vesicle in vivo biodistribution is determined by cell source, route of administration and targeting, J. Extracell. Vesicles 4 (2015) 26316.
[51] J.Y. Wu, Y.J. Li, X.B. Hu, S. Huang, D.X. Xiang, Preservation of small extracellular vesicles for functional analysis and therapeutic applications: a comparative evaluation of storage conditions, Drug Deliv. 28 (1) (2021) 162–170.
[52] Z. Yang, R. Huang, B. Zheng, W. Guo, C. Li, W. He, H. Wang, Highly stretchable, adhesive, biocompatible, and antibacterial hydrogel dressings for wound healing, Adv Sci (Weinh). 8 (8) (2021) 2003627.
[53] M.J. Mitchell, M.M. Billingsley, R.M. Haley, M.E. Wechsler, N.A. Peppas, R. Langer, Engineering precision nanoparticles for drug delivery, Nat. Rev. Mater. 6 (4) (2021) 1078–1094.
[54] Y. Long, L. Yan, H. Dai, D. Yang, X. Wu, X. Dong, Y. Chen, Enhanced proliferation and differentiation of neural stem cells by peptide-containing temperature-sensitive hydrogel scaffold, Mater. Sci. Eng. C Mater. Biol. Appl. 116 (2020) 111258.
[55] X. Qiu, J. Liu, C. Zheng, Y. Su, L. Bao, B. Zhu, Y. Jin, Exosomes released from educated mesenchymal stem cells accelerate cutaneous wound healing via promoting angiogenesis, Cell Prolif. 53 (8) (2020) e12830.
[56] B. Shook, E. Xiao, Y. Kumamoto, A. Iwasaki, V. Horsley, CD301b+ macrophages are essential for effective skin wound healing, J. Invest. Dermatol. 136 (9) (2016) 1885–1891.
[57] S. Babaei, M. Fadaee, H. Abbasi-Kenarsari, D. Shanehbandi, T. Kazemi, Exosome-based immunotherapy as an innovative therapeutic approach in melanoma, Cell Commun. Signal 22 (1) (2024) 527.
[58] L.Y.C. Madruga, K.C. Popat, R.C. Balaban, M.J. Kipper, Enhanced blood coagulation and antibacterial activities of carboxymethyl-kappa-carrageenan-containing nanofibers, Carbohydr. Polym. 273 (2021) 118541.
[59] Z. Ming, L. Han, M. Bao, H. Zhu, S. Qiang, S. Xue, W. Liu, Living bacterial hydrogels for accelerated infected wound healing, Adv Sci (Weinh). 8 (24) (2021) e2102545.
[60] G.Y.C. Cheung, J.S. Bae, M. Otto, Pathogenicity and virulence of *Staphylococcus aureus*, Virulence 12 (1) (2021) 547–569.
[61] T.J. Foster, The MSCRAMM family of cell-wall-anchored surface proteins of gram-positive cocci, Trends Microbiol. 27 (11) (2019) 927–941.
[62] F. Zamboni, C. Okoroafor, M.P. Ryan, J.T. Pembroke, M. Strozyk, M. Culebras, M. N. Collins, On the bacteriostatic activity of hyaluronic acid composite films, Carbohydr. Polym. 260 (2021) 117803.
[63] Y. Yu, H. Jin, L. Li, X. Zhang, C. Zheng, X. Gao, B. Sun, An injectable, activated neutrophil-derived exosome mimetics/extracellular matrix hybrid hydrogel with antibacterial activity and wound healing promotion effect for diabetic wound therapy, J Nanobiotechnology 21 (1) (2023) 308.
[64] K. Zhang, J. Zhu, W. Sun, Y. Zhang, W. Li, Y. Wang, J. Qin, Antibacterial betaine modified chitosan-based hydrogel with angiogenic property for photothermal enhanced diabetic wound repairing, Carbohydr. Polym. 349 (Pt B) (2025) 123033.
[65] J.L. Soriano-Ruiz, A.C. Calpena-Campmany, M. Silva-Abreu, L. Bozal-de Febrer, N. Halbout-Bellowa, M.J. Rodríguez-Lagunas, B. Clares-Naveros, Design and evaluation of a multifunctional thermosensitive poloxamer-chitosan-hyaluronic acid gel for the treatment of skin burns, Int. J. Biol. Macromol. 142 (2020) 412–422.
[66] N.M. King, J. Perrin, Ethical issues in stem cell research and therapy, Stem Cell Res. Ther. 5 (4) (2014) 85.
[67] H.N. Wilkinson, M.J. Hardman, Wound healing: cellular mechanisms and pathological outcomes, Open Biol. 10 (9) (2020) 200223.
[68] Z. Zhu, X. Zhang, H. Hao, H. Xu, J. Shu, Q. Hou, M. Wang, Exosomes derived from umbilical cord mesenchymal stem cells treat cutaneous nerve damage and promote wound healing, Front. Cell. Neurosci. 16 (2022) 913009.
[69] Q. Bai, Q. Gao, F. Hu, C. Zheng, W. Chen, N. Sun, T. Lu, Chitosan and hyaluronic-based hydrogels could promote the infected wound healing, Int. J. Biol. Macromol. 232 (2023) 123271.
[70] J. Huang, X. Lei, Z. Huang, Z. Rong, H. Li, Y. Xie, J. Xia, Bioprinted gelatin-recombinant type III collagen hydrogel promotes wound healing, Int J Bioprint 8 (2) (2022) 517.
[71] L. Diaz-Gomez, I. Gonzalez-Prada, R. Millan, A. Da Silva-Candal, A. Bugallo-Casal, F. Campos, C. Alvarez-Lorenzo, 3D printed carboxymethyl cellulose scaffolds for autologous growth factors delivery in wound healing, Carbohydr. Polym. 278 (2022) 118924.
[72] F. Shams, H. Moravvej, S. Hosseinzadeh, E. Mostafavi, H. Bayat, B. Kazemi, H. Moosavian, Overexpression of VEGF in dermal fibroblast cells accelerates the angiogenesis and wound healing function: in vitro and in vivo studies, Sci. Rep. 12 (1) (2022) 18529.
[73] E. M., A.K. Swaroop, S.K. Patnaik, R.R. Kumar, K.P. T., M.R. Naik, J. S., A novel family of small molecule HIF-1 alpha stabilizers for the treatment of diabetic wounds; an integrated in silico, in vitro, and in vivo strategy, RSC Adv. 12 (48) (2022) 31293–31302.
[74] Y. Hu, S.S. Rao, Z.X. Wang, J. Cao, Y.J. Tan, J. Luo, H. Xie, Exosomes from human umbilical cord blood accelerate cutaneous wound healing through miR-21-3p-mediated promotion of angiogenesis and fibroblast function, Theranostics 8 (1) (2018) 169–184.
[75] P. Martin, R. Nunan, Cellular and molecular mechanisms of repair in acute and chronic wound healing, Br. J. Dermatol. 173 (2) (2015) 370–378.
[76] N. Fortingo, S. Melnyk, S.H. Sutton, M.A. Watsky, W.B. Bollag, Innate immune system activation, inflammation and corneal wound healing, Int. J. Mol. Sci. 23 (23) (2022) 14933.
[77] E. Xiang, B. Han, Q. Zhang, W. Rao, Z. Wang, C. Chang, D. Wu, Human umbilical cord-derived mesenchymal stem cells prevent the progression of early diabetic nephropathy through inhibiting inflammation and fibrosis, Stem Cell Res. Ther. 11 (1) (2020) 336.